SRR-88-03

Ultimate Load Test of a Slab-on-Girder Bridge

Ontario

Ministry of Transportation

Research and Development Branch

Technical Report Documentation Page

Ultimate Load Test of a Slab-on-Girder Bridge

Author:	Baidar Bakht, Principal Research Engineer
Number:	SRR-88-03
Date of Publication:	July, 1988
Ministry Contact:	Baidar Bakht (416) 235-4674
Abstract:	This report describes an ultimate load test on a short-span slab-on-girder bridge with rolled steel girders and a non-composite deck slab, and also presents the relevant data from the test along with the analysis and conclusions drawn. The test was conducted some ten years ago, but could not be reported upon because of apparent discrepancies in the applied moments and the sum of girder moments at the instrumented cross-section computed from measured strains. Since the former is believed to be statically indeterminate in right, simply-supported bridges, the field data was suspected of being inaccurate. Recent tests on similar slab-on-girder bridges have shown that the cause for the apparent discrepancy mentioned above is the presence of fairly large horizontal forces developed due to friction at the interface of the bottom flanges of girders and the surfaces they rest upon. In light of these findings, the test data for the bridge under consideration were re-analysed to find them to be free from any obvious errors. The main conclusions drawn from the test are that: (a) The bearing restraint force reduced the applied moment by a minimum of 11%, (b) The transverse load distribution pattern of the bridge improves at the ultimate limit state, and (c) Any composite action between the deck slab and a girder that may exist at service loads due to bond or friction between steel and concrete completely breaks down as the load approaches the failure load for the girder under consideration.
Comments:	
Key words:	bearing restraint, composite action, evaluation, load distribution, slab-on-girder bridge, steel girders, testing, ultimate load test
Distribution:	MTO Head Office and Regions, selected structural engineers around the world, and upon request.
Copyright Status:	Crown copyright © 1988 Ministry of Transportation

SRR-83-03

Ultimate Load Test of a Slab-on-Girder Bridge

B. Bakht
Principal Research Engineer
Structures Research Office
Research and Development Branch

Published by
The Research and Development Branch
Ministry of Transportation of Ontario
Hon. Ed Fulton, Minister
D.G. Hobbs, Deputy Minister

Published without prejudice as to the application of the findings.
Crown copyright reserved; however, this document may be reproduced for non-commercial purposes with attribution to the Ministry.

For additional copies, contact:
The Editor, Technical Publications
Room 320, Central Building
1201 Wilson Avenue
Downsview, Ontario
Canada M3M 1J8

Telephone: (416) 235-4704
CNCP Dialcom Electronic Mail: 23:MIN006

July 1988

Table of Contents

List of Tables and Figures iii

1. Test Summary 1

2. Introduction 2

3. Bridge Description 4

4. Testing Procedure 5
4.1 Preparing the Bridge for the Test 5
4.2 Instrumentation 5
4.3 Loading 6
4.4 Definition of Failure 7

5. Recorded Data 8
5.1 Girder Strains 8
5.2 Girder Deflections 9
5.3 Interface Slip 9
5.4 Cracking of the Deck Slab 10

6. Interpretation of Girder Strains 12
6.1 Analytical Procedure for Obtaining Girder Moments 12
6.2 Calculated Responses 16
Bearing Restraint Forces 17
Transverse Distribution of Girder Moments 18
Neutral Axis Positions 20

7. Summary of Conclusions 21
Global and Local Failure 21
Cracking of the Deck Slab 21
Bearing Restraint Force 21
Load Distribution at Service Loads 22
Load Distribution at Ultimate Limit State 22
Composite Action 22

8. References 23

List of Tables and Figures

Tables

5.1 Longitudinal strains in girders at mid-span due to loading in the southern segment of the bridge 24
5.2 Longitudinal strains in girders at mid-span due to loading in the southern segment of the bridge 25
5.3 Relationships between local and overall failure loads 26
5.4 Mid-span deflections of girders 27
5.5 Values of interface slip between the deck slab and top flanges of girders, near the eastern abutment 28
6.1 Total net moments in girders at mid-span 29
6.2 Distribution factors for girder moments at mid-span 30

Figures

2.1 Views of the Stoney Creek Bridge a few months before the test 31
2.2 Moments at mid-span due to one particular load case 32
3.1 Bridge details 33
4.1 A view of the bridge showing a part of the temporary wood structure erected under the bridge 34
4.2 Gauges at or near mid-span and their identifying numbers 35
4.3 Instruments for measuring interface slip 36
4.4 Placing sequence of loading in the southern segment of the bridge 37
4.5 Beam moments at mid-span 38
4.6 Loading of the bridge with concrete blocks 39
4.7 Placing sequence of loading in the northern segment of the bridge 40
4.8 Placing of concrete blocks in the 7th layer for loading in the southern segment 41
4.9 Girder deflections at mid-span 42
5.1 Some girder strains plotted against load 43
5.2 Interface slip of deck with respect to the top flange of girders 44
5.3 Exaggerated representation of interface slip 45
5.4 Crack pattern due to ultimate load on the southern segment of the bridge 46
5.5 Crack pattern due to ultimate load on the northern segment of the bridge 47
5.6 An element of deck slab 48
6.1 Calculation of girder moments from measured strains 49
6.2 Girder moments at mid-span due to loading in southern segment 50
6.3 Girder moments at mid-span due to loading in northern segment 51
6.4 Reduction of applied moments due to bearing restraint 52
6.5 Ratios of restraint force to total reaction 53
6.6 Transverse distribution of girder moments due to loading in southern segment 54
6.7 Transverse distribution of girder moments due to loading in southern segment 55
6.8 Variation in values of maximum distribution factors for moments with respect to load level 56
6.9 Positions of neutral axes 57
6.10 Positions of neutral axes 58

1. Test Summary

Bridge:	Stoney Creek Bridge, City of London Site No. 19-252
Type of Bridge:	Slab-on-girder with six rolled steel girders and a concrete deck slab without any mechanical shear connection between the girders and the deck slab.
Posted Weight:	None
Span/Width:	13.72/6.33 m
Angle of Skew:	0 degrees
Dates of Test:	May 15 and 16, 1978
Test Engineer:	Baidar Bakht
Job Captain:	Zdislaw Knobel
Supervisor Instrumentation:	Wayne Wagner
Failure Load:	1418 kN applied centrally over a length of about 4.88 m, and transversely over a width of about 3.67 m.
Responses monitored:	Longitudinal strains in girders at mid-span, deflections of the two outer girders at mid-span, and relative slip of the top flanges of girders with respect to the deck slab near one abutment.
Main observation:	Bearing restraint at the bottom flanges of girders reduced the total applied moments by a minimum of about 11% and a maximum of about 18%.

2. Introduction

The Stoney Creek bridge in the City of London was a right, short-span, two lane bridge with a concrete deck slab and six rolled steel girders which were "simply supported" on concrete abutments. The 40-year-old bridge, while being in relatively good shape, was scheduled to be removed in 1978 for replacement by a wider bridge. The existing bridge was offered to the Structural Research Office of the Ministry of Transportation of Ontario (MTO) for a test to failure. Two photographs of the bridge taken a few months before the test, are shown in Figs. 2.1 (a) and (b).

The ultimate load that was conducted in May 1978 by loading the bridge with concrete blocks as described later in Chapter 4. The purpose of the test was to study the transverse load distribution pattern of the slab-on-girder bridge at the ultimate limit state, and to examine the degree of composite action at different load levels between the girders and the apparently non-composite deck slab. Following the customary practice at the time of the test, the instrumentation was designed to measure mainly the longitudinal girder strains at mid-span.

The analysis of the test data started a few months after the test. The first check on the validity of the test data consisted of calculating girder moments at various load levels at the instrumented mid-span from the measured strains, and then comparing the sum of calculated girder moments with the corresponding applied moments. It is noted that the latter moments are supposed to be statically determinate at any transverse section in a truly right, simply-supported bridge. Further, as shown later in the report, there is little room for error in the calculation of girder moments in a simply-supported bridge from girder strains, provided, of course, that the strains are correct. In these calculations, following the customary practice, it was assumed that the girder cross-sections were free from any externally applied loads.

These calculations showed that for every load case, the sum of girder moments at mid-span computed from measured strains was generally about 30% smaller than the applied moments. To illustrate this point, example is given of the loading case in which the loading comprised concrete blocks in only one layer. For such loading, the concrete blocks cannot be suspected of interlocking and influencing the pattern of loading on the bridge. The computed girder moments for the case under consideration, are plotted in Fig. 2.2, which also shows the average applied moments and the average computed moments. In ideal circumstances, the two averages should be nearly the same. However, for the example of Fig. 2.2, the average of computed girder moments was found to be about 28% smaller than the average applied moment. This kind of discrepancy casts serious

doubt on the accuracy of the measured data, especially when the measured strains are well within the elastic range.

Unfortunately, the strains of the bottom flanges of girders were not measured near the abutments, because of which no data were available for the horizontal force that may have developed due to friction between the bottom flanges of steel girders and the concrete abutment. These forces, which are termed as the *bearing restraint forces*, were initially dismissed as being the cause for the discrepancies mentioned above. This was because bearing restraint forces of such large magnitude as to reduce the applied moments by up to 30% were believed to be unlikely to develop in practice.

Since the test on the Stoney Creek bridge, numerous futile attempts were undertaken to either establish the causes for the reduction of applied moments, or to find the source of error in measured data.

The reasons for the apparent discrepancy between the applied moments and those calculated from the test data, were established conclusively by the several tests on slab-on-girder bridges undertaken during the past two years by the Structural Research Office of the MTO. It was found that the "simply-supported" bridges were not really simply supported, and that the bearing restraint force was primarily responsible for apparently stiffening these bridges. It was also found that neglecting the effects of bearing restraint forces in the calculation of girder moments from measured strains, leads to significant underestimation of moments (see e.g. Bakht, 1988a and b).

In light of the knowledge gained from the tests mentioned above, the data from the ultimate load test on the Stoney Creek bridge, were re-analysed by back-calculating the bearing restraint forces that may have occurred. This time it was found that the applied moment was reduced by the bearing restraint force by 11 to 18%, and not 30%, as was wrongly shown by the previous calculations. This kind of reduction in applied moments is consistent with the observations from other tests on similar bridges.

The data from the ultimate load test on the Stoney Creek bridge, and their analysis, are now presented in this report some ten years after the last test, but with full confidence in the reliability of the data and the conclusions drawn therefrom.

The purpose of this report is to record the description of the test and its relevant data, and to present the analysis of the data along with the conclusions drawn from the test.

Note about Graphical Presentation of Girder Responses: Whenever girder responses, such as moments and deflections, are presented graphically in this report across a transverse section, the discrete values of the responses are joined by a continuous smooth curve as in Fig. 2.2. This is done to facilitate the inspection of the transverse pattern, and not to imply that these responses are continuously distributed in the transverse direction.

3. Bridge Description

The Stoney Creek bridge was located on Fanshawe Park Road in the north east of the City of London, Ontario; it was a 40 year old, right, single-span, two-lane bridge with a clear span of 13.72 m and a width of 6.33 m. The bridge consisted of six rolled steel girders of W610 x 110 section and a concrete slab which varied in thickness from about 180 to 195 mm. The thickness of the asphalt layer over the deck slab varied between 95 and 130 mm. There was no mechanical shear connection between the deck slab and the girders. However, the top flanges of the girders were partially imbedded in concrete so that their bottom surfaces were generally flush with the underside of the deck slab.

The concrete of the deck slab, as viewed from the underside was free from cracks, and generally sound except over the two outer girders. In those regions, the concrete appeared deteriorated and the top flanges of girders rusted.

The steel girders rested directly on the concrete abutments which appeared to be sound and generally free from cracks. There were very small, yet usually clear, gaps between the girders and the ballast walls. However, the asphalt layer was continuous over the gap, so that no gap was visible from the road surface.

The cross-section and plan of the bridge are shown in Fig. 3.1 which also shows the details of a typical girder support and of the cross-section of a rolled steel girder. The cross-section of the rolled steel girder is identified in Imperial units as 24 WF x 74. Relevant details of this section, which are no longer generally available, are also given in Fig. 3.1.

The bridge had a one metre wide sidewalk on either side. These sidewalks, which were clearly added after the construction of the bridge, consisted of wood planks resting on light steel brackets framing out of the outer girders. There were wire mesh railings towards the outsides of the sidewalks and slightly heavier railings were provided directly over the outer girders to separate the

sidewalks from the main roadway. Since the light wood planks of the sidewalks were not expected to have participated, even in a small way, towards the bridge strength, they are omitted from the relevant figures given in this report.

4. Testing Procedure

4.1 Preparing the Bridge for the Test

The main railings of the bridge which separated the sidewalks from the roadway and which can be seen in Fig. 2.1 (a), were removed before the test so as not to interfere with the interpretation of the test data. However, the wire mesh railings of the sidewalks were left intact. The creek that flowed under the bridge had already been diverted away from the bridge before the test, in preparation for the new construction. For the test, the creek channel under the bridge was levelled by gravel to provide a level surface about 1.5 m below the bridge girders. A wood structure, a part of which can be seen in Fig. 4.1, was erected on this level surface to prevent the bridge from deflecting catastrophically at failure. The wood structure was erected near mid-span of the bridge; a gap of about 110 mm was maintained between the top of the wood structure and the bottom of the girders, before any loading was applied to the bridge.

4.2 Instrumentation

Longitudinal strains of the girders at mid-span were measured by three uni-directional electrical resistance strain gauges on each girder. As shown in Fig. 4.2, one gauge was located at the underside of the bottom flange, one midway between the two flanges on the web, and another also on the web, but about 50 mm below the underside of the top flange. Also as shown in Fig. 4.2, deflections near mid-span of the two outer girders were measured by means of deflection transducers which were secured to the temporary wood structure underneath the bridge. One of the deflection transducers can be seen in Fig. 4.1. The identifying numbers of the various gauges at and near mid-span are also shown in Fig. 4.2.

Near the east abutment, special brackets were attached to the underside of the deck slab and top flanges of girders. As shown in Fig. 4.3, deflection transducers were attached to pairs of brackets to measure longitudinal slip of the deck slab with respect to the top flanges of the girders. The locations, and identifying numbers of these instruments are also shown in Fig. 4.3.

4.3 Loading

It was decided to load the bridge by means of concrete blocks. These concrete blocks, each of which weighs about 9.26 kN, are used regularly for bridge testing in Ontario. Each block measures about 0.61 x 1.22 m on the plan, and is 0.61 m high. Two hooks are attached on the top of each block to facilitate lifting. There are mating recesses on the underside of each block to accommodate these hooks so that the blocks can lie flat on top of each other.

The loading was planned to be applied over a 4.88 x 3.67 m area which was symmetrical about the mid-span line, but was eccentric transversely so that it was flush with the southern curb of the bridge. The order of placing the blocks in each layer, which contained 24 blocks, was pre-decided and was as shown in Fig. 4.4. The blocks in different layers were arranged so as to interlock to safeguard against the possibility of their falling over from the pile as bridge deflections increase. The interlocking of the blocks was tolerated even at the expanse of possible errors that may be introduced due to uncertain distribution of loads as the deflections of the bridge become excessive. However, as shown below, the errors introduced due to changes in the pattern of loading were expected to be relatively small.

If the loading were distributed uniformly, the total mid-span moment in the bridge treated as a simply-supported beam would be 2.82 W, as shown in Fig. 4.5 (a), where W is the total load on the beam. In Fig. 4.5 (b), the same total load W is shown distributed in a double triangular fashion so the load intensity is maximum at the edges decreasing linearly to zero at mid-span. In this second unlikely and extreme case, which may happen only if the bridge deflections become excessively large and the concrete blocks interlock, the mid-span moment is 2.62 W, or only 8% smaller than the corresponding moment in the previous case. It was expected that in practice the loading patterns would be closer to that shown in Fig. 4.5 (a), than the pattern shown in Fig. 4.5 (b). Accordingly, the errors incorporated by the interlocking of the blocks were expected to be extremely small.

For loading the bridge with concrete blocks, two cranes, both stationed well away from the bridge, were employed. One crane was used to lower a concrete block at the stated position, and the other carried two buckets with a person in each, one of whom manoeuvred the block so that the hooks and recesses of overlying blocks mated snuggly and the other operated the crane. The buckets carrying the two persons were always kept well above the pile of concrete blocks so that in the unlikely event of the pile toppling over, the persons in the bucket remained unharmed. The

process of loading by using two cranes can be seen in the photograph given in Fig. 4.6. In the right-hand corner of the photograph can be seen the front-end of the crane lowering the blocks.

For the loading sequence shown in Fig. 4.4, the bridge was declared to have failed after the ninth block was placed in the seventh layer, i.e. after 153 blocks. When all the blocks were removed after the test, the bridge sprang back to such a position that it could have been used again to carry traffic. It was decided to retest the bridge with the loading moved over to the northern segment. The position of load in the second case, which was not originally planned, is shown in Fig. 4.7. Loading in the former case is referred to in this report as "loading in the southern segment", and that in the latter as "loading in the northern segment".

It is noted that for loading in the northern segment, the bridge was declared as having failed after the eleventh block was placed in the seventh layer, i.e. after 155 blocks. A view of the bridge is shown in Fig. 4.8 with blocks being placed in the seventh layer in the first loading sequence.

4.4 Definition of Failure

By erecting the temporary wood structure under the bridge, it was made certain that the girder deflections at mid-span would not be allowed to exceed about 110 mm. This limitation on deflection was dictated by the need to avoid a catastrophic failure in which the concrete blocks by being thrown away from the bridge were likely to be damaged requiring an extra sum of money for the "clean up" after the test. Fortuitously, however, these limits on the deflection were also compatible with the load capacity limit as decided upon by the load-deflection curves.

The load-deflection curves for the two outer girders corresponding to the two loading sequences are shown in Fig. 4.9. The curves for the more heavily loaded girders could be plotted only up to those points at which the girder deflections were interrupted by the temporary wooden structure below the bridge. Beyond the points, the curves are projected to becoming asymptotic to the deflection axis. From these projected curves, it can be confirmed that the loads to cause infinitely large deflections, i.e. the failure loads, are only slightly higher than the loads which caused the limiting deflections. In fact, it appears that if it were not for the temporary wood structure under the bridge, the bridge may have had overly excessive deflections even under the maximum applied load levels.

5. Recorded Data

Readings from all the instruments were recorded after every twelve concrete blocks were placed up to the third layer of loading. Subsequent to that level of loading, the readings were taken after placing every six blocks. Since the patterns of readings did not change suddenly, or unusually, with the load, it is considered sufficient to record the instrument output corresponding to the completion of loading in each layer. The data presented herein has the zero readings, i.e., the readings before the application of loads, deducted from them. It is, indeed, assumed that during the course of each loading sequence the gauges did not drift sufficiently to affect significantly the final readings. The assumption that the gauges did not drift was confirmed to be valid by readings from the several "dummy" gauges which were found to be quite stable.

5.1 Girder Strains

Readings of longitudinal girder strains at mid-span due to loading in the southern segment are given in Table 5.1 in micro-strains, i.e. in mm x 10^{-6}/mm. As noted in the table, the tensile strains are shown as positive and, indeed, the compressive strains as negative. Girder strains at mid-span due to loading in the northern segment are recorded in Table 5.2. Some of the highest girder strains are plotted against load level in Fig. 5.1, which also shows the elastic limit for strains due to applied moments. The limit was obtained by deducting the strains due to dead load stresses in the girder flanges, being equal to about 70 MPa, from the assumed yield stress in the girder steel of about 228 MPa.

It can be seen that the applied load causing failure in an individual girder is much higher than the load causing the girder to first yield. Also, it is obvious that the bridge continues to carry loads long after the failure of individual girders.

For example, for the loading in the southern segment, strains in the top flanges of girder No. 1 reach the elastic limit with loading in about 4.5 layers, and fails with loading in about 5.5 layers. For the loading sequence under consideration, the bridge failed with loading in about 6.4 layers. It can be summarized that for this case, the ratio of loads to cause overall failure and local failure in an outer girder is about 1.40. Similarly, for the same case, the ratio of loads to cause failure of the outer girder and to cause first yield in the same girder is 1.20. Similar and other ratios, rounded to 5th percentile, are given in Table 5.3 for some other cases as well. The ratios of overall and local failure loads presented in this table underline the random nature of the bridge capacity. It can be

seen that these ratios cannot apply to even the same bridge if the load positions are altered symmetrically.

Scrutiny of the numbers given in Table 5.3 and of the load-strain curves presented in Fig. 5.1, will readily show the lack of correspondence in the bridge behaviour due to the two symmetrical loading cases. It seems that the closeness of the failure loads corresponding to the two loading sequences was just a coincidence.

The ratios listed in Table 5.3 confirm that the overall failure load is much greater than the load causing failure of the first girder, and even greater than the loading causing first yield in a girder.

5.2 Girder Deflections

Due to the limited number of channels available on the data acquisition system, it was decided to measure only the deflections of the two outer girders. Besides recording these deflections, at the end of different loading sequences, they were also continuously recorded on a strip chart recorder to provide a visual aid in monitoring and controlling the test from inside the mobile laboratory which was stationed close to the bridge.

The mid-span deflections of the two outer girders due to the various loading cases are listed in Table 5.4. These deflections are already plotted against load level in Fig. 4.8. It is interesting to note that when the bridge was loaded in the southern segment, the outer girder remote from the loading had a downward deflection until the load nearly reached the failure load level. For the loading in the northern segment, on the other hand, the outer girder remote from the loading had an upward deflection from the start; it also had negative moments as indicated by tensile strains in the top flanges and compressive in the bottom. These reverse strain patterns can be seen in Table 5.2.

Although the outer girders remote from the applied loading seemed to have behaved differently, their load-deflection patterns are remarkably similar, as can be seen in Fig. 4.8.

5.3 Interface Slip

The relative movement of deck slab with respect to the top flanges of the girders, termed as the "interface slip", was measured above all the girders close to the eastern abutment of the bridge; it is noted as positive if the relative movement of the deck slab is towards the abutment. Values of interface slip after loading in each layer, are listed in Table 5.5.

Interface slip above the two most heavy loaded girders in each loading sequence, are plotted in Fig. 5.2 against loads. A comparison of load-deflection curves, plotted in Fig. 4.6, with the curves shown in Fig. 5.2 will readily show similarities in patterns of behaviour of the two responses. Other observations regarding the measured interface slip data are offered in the following.

From the curves plotted in Fig. 5.2, it is obvious that for a given load level, the interface slip is the smallest in girder No. 2, indicating that in this girder the degree of composite action is the highest. This observation is supported by the fact that, as can be seen in Tables 5.1 and 5.2, the differential of absolute strains in the top and bottom flanges for the same load level, is higher in girder No. 2 for south loading than for its counterpart, i.e., girder No. 5 for north loading. Accordingly, the failure load as projected from the load-interface slip curves is higher for the former case than for the latter.

The interface slip for girder No. 6 due to loading in the northern segment is positive and increasing until loading at the end of load layer No. 2. Thereafter, the value remains constant until after load layer No. 4, it starts decreasing to become negative after load layer No. 5. This kind of behaviour, while appearing at a cursory glance contrary to engineering judgement, can be rationalized by noting that after loading in the third layer, the composite action breaks down completely in girder No. 6, but is retained to a certain degree in the neighbouring girders. The very large bottom flange strains in girder No. 5 after loading in the third layer (shown in Table 5.2) indicate excessive deflections in this girder. Such girders with partial composite action and large deflections are likely to force the edge of the deck slab near the abutments to such a position that an adjacent girder with no composite action and relatively smaller deflections can develop a negative interface slip. This process is illustrated in Fig. 5.3 (a) and (b), where the former figure shows a girder like No. 5 under loading in the northern segment, and the latter a girder like girder No. 6 under the same loading. With the help of these figures it can be readily appreciated that the negative interface slip over girder No. 6 as shown in Fig. 5.2 is a reliable recording of actual behaviour and is not the result of instrument malfunction.

5.4 Cracking of the Deck Slab

When the deck slab was inspected from the underside after the removal of loading in the southern segment, it was discovered that it had developed a systematic crack pattern which was symmetrical about the mid-span line. The crack pattern was mapped carefully for one half of the span, and is shown to scale in Fig. 5.4. Only those cracks are shown in this figure which were visible to the

naked eye from a distance. It can be seen in Fig. 5.4 that the cracks run at 45° from the girder axes, and are contained between the girders carrying the applied load directly. The fact that these cracks do not cross over the girder locations, suggests that the forces causing them to develop are local to deck slab panels between two adjacent girders.

After the test with loading in the northern segment, the deck slab was inspected again from the underside for cracks. It was found that the new pattern of cracks was complementary to that developed after loading in the southern segment. The new crack pattern is shown in Fig. 5.5, again for one-half of the bridge. A comparison of Figs. 5.4 and 5.5 will readily confirm the similarities between the two crack patterns.

By isolating a rectangular segment of the deck slab, it can be shown that cracks of the type observed in practice can develop by distorting the slab in plan as shown in Fig. 5.6. This kind of distortion of the deck slab can be explained as follows if there is some composite action between the deck slab and the girders.

Consider a point in the deck slab at the interface of the slab and a girder. In the absence of any composite action between the deck slab and the girder, let this point assume position P identified in Fig. 5.3. With any composite action between the slab and the girder, the compressive strains in the top flange of the girder will force point P to move towards mid-span to point P' also shown in Fig. 5.3. For a given degree of composite action the distance PP' will depend upon girder deflections. The larger the deflections, the larger will be this distance. In light of this conclusion, now consider the deck slab segment ABCD, shown in Fig. 5.6, contained between girder Nos. 1 and 2 with the deflections of the former being larger than those of the latter. It can be readily appreciated that point A over the girder with larger deflections will move closer to mid-span than the corresponding point over the next girder, thus distorting the segment of slab as shown in Fig. 5.6, and causing it to crack in the pattern as observed in the field.

The crack patterns shown in Figs. 5.4 and 5.5 show a failure mode of the deck slab in a composite slab-on-girder bridge which is usually not accounted for in the deck slab design.

6. Interpretation of Girder Strains

6.1 Analytical Procedure for Obtaining Girder Moments

The total moment M taken by a fully, or partially composite girder can be divided into M_L, M_u and Na, where M_L and M_u are moments taken the steel girder alone and the concrete flanges, respectively, bending about their own axes. N is the axial force acting in opposite directions in the girder and concrete flange to a lever arm "a". Thus, the moment M taken by the composite girder is given by:

$$M = M_L + M_u + Na \tag{6.1}$$

The process of obtaining M by Eq. (6.1) is illustrated schematically in Fig. 6.1 (a).

As shown by Bakht (1988 a), the various terms on the right-hand side of Eq. (6.1) can be obtained as follows:

$$M_L = \sigma_{fb} S_b \tag{6.2}$$

$$M_u = M_L (EI_s/EI_g) \tag{6.3}$$

$$Na = \sigma_a A a \tag{6.4}$$

where

- σ_{fb} = flexural stress in the bottom flange of the steel girder.
- S_b = section modulus of the naked steel girder with respect to the bottom flange.
- EI_g = flexural rigidity of the naked steel girder bending about its own neutral axis.
- EI_s = flexural rigidity of the portion concrete slab associated with the girder, bending about its own axis.
- σ_a = axial stress in the naked steel girder due to axial force N
- A = area of cross-section of the naked steel girder
- a = lever-arm of the couple due to axial forces N

It is sufficiently accurate to assume that the lever-arm a is equal to the distance between the neutral axes of the concrete flange and the steel girder.

When the section is free from any external axial forces, such as those induced by the bearing restraint, σ_{fb} and σ_a can be computed directly from the stresses obtained from measured strains in the top and bottom flanges of girders. Since M_u is generally very small as compared to M_L and Na, any possible error incurred by a wrong estimate of the modulus of elasticity of the deck slab concrete is likely to affect M only slightly.

In the presence of axial forces induced by the bearing restraint, σ_{fb} and σ_a should be obtained from the measured strain data by accounting for these axial forces. This can be done as follows:

Let the stresses computed from measured strains in the top and bottom flanges of the girder at the section under consideration be designated as σ_t' and σ_b', respectively, as distinct from σ_t and σ_b which are the top and top and flange stresses, respectively, in the absence of externally applied axial forces. Further, let the external force be denoted as F. The average axial stress σ_{as} due to bearing restraint is obtained by dividing F with the effective cross-sectional area A of the composite section.

$$\sigma_{as} = F/A_c \tag{6.5}$$

In the case of a fully composite section, A_c can be calculated readily after a value of the modular ratio is assumed. However, for partially composite bridges such as the one under consideration, it is difficult to assess A_c which for the sake of convenience is assumed to be equal to the area of cross-section of the steel girder alone.

If the value of F, and hence σ_{as}, is known, the following expressions can be used to calculate σ_t and σ_b.

$$\sigma_t = \sigma_t' - \sigma_{as} \tag{6.6}$$
$$\sigma_b = \sigma_b' - \sigma_{as} \tag{6.7}$$

The process of obtaining σ_t and σ_b from stress calculated from measured strains is illustrated in Fig. 6.1 (c). The expressions for obtaining σ_{fb} and σ_a are as follows:

$$\sigma_{fb} = 0.5\ (\sigma_b - \sigma_t) \tag{6.8}$$
$$\sigma_a = 0.5\ (\sigma_b + \sigma_t) \tag{6.9}$$

The unknown value of the bearing restraint force can be determined approximately as follows from stresses computed from measured top and bottom flange girder strains at a transverse section and the known applied moment at the same section, obtained by treating the bridge as a simply-supported beam.

It is assumed that the sum of restraint forces in all girders, designated as F', can be determined realistically from the sums of top flange and bottom flange stresses in all girders, denoted as σ_T' and σ_B', respectively. This assumption was found to be valid within reason from a large number of checks using data reported by Bakht (1988 a and b). From the observed data, values of the bearing restraint forces could be obtained realistically, which compared fairly well with those obtained by the procedure given below. It is noted that this procedure is based upon the assumption stated above. Further, it is assumed that the girders are supported at the neutral axis locations at their ends, so that the girder moments calculated in the following correspond to the moments at the neutral axis locations.

Using the equations given above, M_L, M_u and Na can be shown to be given by:

$$M_L = 0.5\,(\sigma_B' - \sigma_T')\,S \tag{6.10}$$

$$M_u = M_L\,(EI_s / EI_g) \tag{6.11}$$

$$Na = 0.5\,(\sigma_B' + \sigma_T' - 2\sigma_{as})\,Aa$$

where σ_{as} is determined from Eq. (6.2) by replacing F with F'. The distance of the neutral axis from the bottom flange, designated $\bar{y}$, is given by:

$$\bar{y} = D\left\{\frac{\sigma_B' - \sigma_{as}}{\sigma_B' - \sigma_T}\right\} \tag{6.12}$$

where D is the girder depth.

If M is the applied moments at the section under consideration obtained by treating the bridge as a simply-supported beam, then the net moment M' at the section is given by:

$$M' = M - F'\,\bar{y} \tag{6.13}$$

Or, by substituting the expression for $\bar{y}$ from Eq. (6.12) into Eq. (6.13):

$$M' = M - \sigma_{as} A_c D \left\{ \frac{\sigma_B' - \sigma_{as}}{\sigma_B' - \sigma_T} \right\} \tag{6.14}$$

The net moment M' is also equal to the sum of M_L, M_u and Na, i.e.:

$$M' = M_L + M_u + Na \tag{6.15}$$

By equating the right-hand sides of Eqs. (6.14) and (6.15), and rearranging, the following equation is obtained.

$$- \frac{AD}{(\sigma_B' - \sigma_T')} \sigma_{as}^2 + \left\{ Aa + \frac{AD\sigma_B'}{\sigma_B' - \sigma_T'} \right\} \sigma_{as}$$

$$+ M - \frac{(1 + k)}{2} S_b (\sigma_B' - \sigma_T') - \frac{(\sigma_B' - \sigma_T')}{2} Aa = 0.0 \tag{6.16}$$

where

$$K = EI_s / EI_g \tag{6.17}$$

Eq. (6.16) can be solved for σ_{as} to give:

$$\sigma_{as} = \frac{-X_2 \pm \sqrt{X_2^2 - 4X_1X_3}}{2X_1} \tag{6.18}$$

where

$$X_1 = \frac{-AD}{(\sigma_B' - \sigma_T')} \tag{6.19}$$

$$X_2 = Aa + \frac{AD\sigma_B'}{(\sigma_B' - \sigma_T')} \tag{6.20}$$

$$X_3 = M - 0.5S_b (\sigma_B' - \sigma_T') (1 + K) \tag{6.21}$$

After obtaining the value of σ_{as}, and hence of F', there remains the matter of apportioning the bearing restraint force to the various girders. In the absence of the relevant experimental data, the bearing restraint force was distributed to the various girders in proportion of their measured bottom flange strains at mid-span.

Having approximately calculated the value of σ_{as} for each girder, the moment taken by the girder and the associated portion of the deck slab can be calculated by using Eqs. (6.1) through (6.8).

As long as the strains are within elastic limits, stresses can be obtained from measured strains by multiplying them with the modulus of elasticity of steel which was assumed to be equal to 200,000 MPa. However, when the strains exceed the elastic limit, which is identified in Fig. 5.1, the interpretation of data by the procedure given above, no longer remains ever approximately valid. In such cases, the girder moments were computed by considering the moments taken by the girder in previous load cases which induced strains within the elastic range, and also by taking account of the moments in adjacent girders at least three of which had strains within elastic limits even at the ultimate load level.

As shown in Fig. 5.1, the limit of elastic strains in the bottom flanges of the various girders, after accounting for the dead load effects, was about 750 x 10^{-6} mm /mm. Table 5.1 shows that this limit was rarely exceeded in girder Nos. 4, 5 and 6 for loading in the southern segment. Similarly, as can be seen in Table 5.2, the strains in the bottom flanges of girder Nos. 1, 2, 3 and 4 never exceeded the elastic limits for loading in the northern segment. Moments in these girders, which could be calculated relatively accurately were used with advantage to establish the remaining moments that would have been shared by the girders whose strains exceeded the elastic limit.

It should be noted that all the bottom flange strains remained within the elastic limit up to the fourth layer of loading in the southern segment and up to the third layer of loading in the northern segment. Up to these levels, the calculated girder moments are fairly reliable. However, beyond these levels the computed moments are no longer as reliable. They should be taken as indicative of trends rather than absolute values.

6.2 Calculated Responses

Girder moments computed from measured strains by the procedure given in Section 6.1, are plotted in Fig. 6.2 for various load levels due to loading in the southern segment. Similar plots of moments due to loading in the northern segment are given in Fig. 6.3. It can be seen that the

patterns of transverse distribution of girder moments are not irregular or contrary to engineering judgement, thus validating, to a certain extent, the accuracy of calculations. However, a better test of the accuracy of calculations is provided by comparing the applied moments with the sum of computed girder moments. Details of such a check are provided in the following:

Bearing Restraint Forces

The total net applied moments in the bridge at a given section at the neutral axis location are equal to $M + F' \bar{y}$, where M is the beam moment obtained by treating the bridge as a simply-supported beam; F' is the total bearing restraint force and $\bar{y}$ is the effective distance of the neutral axis from the bottom flange at the section under consideration as obtained by Eq. (6.11). Since the value of F' was found negative in all cases, the net effect of the bearing restraint was to reduce the beam moment by $F' \bar{y}$. If the calculations are correct, the ratio of the sum of computed girder moments, denoted as $\bar{M}$, to $M + F' \bar{y}$ should be very nearly equal to 1.0. This is, indeed, the case as shown in Table 6.1 in which the net applied moments are compared with the sum of computed moments. A close comparison of net applied moments with the sum of computed girder moments confirms the numerical accuracy of the calculations.

Table 6.1 also lists the values of $F' \bar{y}$, for the various cases and the ratio ($F' \bar{y}/M$) which indicates the degree of reduction of applied moments by the bearing restraint. These ratios are plotted against load level in Fig. 6.4 for the two loading sequences. It can be seen that as loading in the southern segment increases, the ratio ($F' \bar{y}/M$) decreases gradually from about 16 to 11%. The same kind of trend can be observed for loading in the northern segment, except that the ratio increases as the loading increases from the third to the fifth layer. Thereafter, the trend of reduction is similar to that observed for the former loading.

The ratios of computed restraint force F and the total applied and dead load reaction, designated as μ, at the abutment are plotted in Fig. 6.5 against the load level for the two loading sequences. It can be seen that for higher load levels, this ratio becomes asymptotic to 1.0 for loading in the southern segment, suggesting that the bearing restraint force is developed only due to friction, and that the effective value of the coefficient of friction between the girder and its support is nearly equal to 1.0.

For up to load layer No. 3 in the northern segment, the value of μ is nearly the same as in the other loading sequence, but for higher loads it starts increasing rapidly. This rapid increase in the value of μ to up to about 1.7 indicates that in this sequence of loading, the total bearing restraint force

after the third layer of loading is no longer caused by friction alone. It is conceivable that the small gap between the bottom flanges of the most heavily loaded girders, such as Nos. 1 and 2, and the ballast walls closed completely after loading beyond load layer No. 3, forcing these flanges to bear against the ballast walls and thus develop the higher bearing restraint forces. Such behaviour cannot be regarded as typical.

Transverse Distribution of Girder Moments

The transverse plots of mid-span girder moments given in Figs. 6.2 and 6.3 do seem to suggest qualitatively that the pattern of transverse distribution of girder moments is not significantly affected by the load level. For a qualitative assessment, it is necessary, however, to scrutinize the distribution factors (DF) which for a given response are the dimensionless ratios of the actual to average responses.

The DF for mid-span girder moments computed from the field data, are given in Table 6.2 for different load levels in both the loading sequences.

The DF for mid-span moments corresponding to the loading in the southern segment, are plotted in Fig. 6.6 for load layer Nos. 1, 2, 5 and 6. This figure also has the load-deflection curve for girder No. 1 to provide a ready reference for establishing if a load level is in the linear or non-linear range of behaviour. It can be seen that in spite of the fact that the bridge behaviour is linear up to the third layer of loading, the patterns of transverse distribution of moments are not exactly the same for loadings up to layer Nos. 1 and 2. In fact, the maximum DF for the latter case is about 3.5% larger than that for the former.

The steepening slope of load-deflection curve corresponding to load layer Nos. 5 and 6, clearly indicates that these load levels are not far below the failure load. For these load levels, as can be seen in Fig. 6.6, the load tends to get slightly more evenly distributed in the transverse direction, with the maximum DF corresponding to load layer No. 6 being about 12.5% smaller than that corresponding to load layer No. 1.

It is interesting to note that throughout the loading in the southern segment, the girder most remote from the applied loading (girder No. 6) attracted so little moments that even if the girder were removed, the pattern of transverse distribution of load would have been hardly affected. This is a very significant observation as it means that the redistribution of loads, which led to a decrease of 12.5% in the DF for maximum moments, took place only within the immediately loaded girders

and one more. Or, in other words, such a reduction in maximum DF for moments took place when about 75% of the bridge width was covered by a uniformly-distributed load. If this two-lane bridge were loaded by two, side-by-side vehicles, instead of a uniformly distributed load, there would have been slightly more room for transverse redistribution of moments, and accordingly the reduction in the maximum DF corresponding to the failure load would have been somewhat larger.

The DF for mid-span girder moments corresponding to loading in the north segment are plotted in Fig. 6.7 for the same load levels for which the DFs are plotted in Fig. 6.6. It can be shown that in this case the reduction in the maximum value of DF by going from load in the first layer to the sixth is only about 5.5%. It can also be seen that in this case as well, the girder most remote for the applied loading (girder No. 1) carried so little moments that it could have been eliminated without affecting the outcome, even slightly.

The effect of load level on the values of the maximum DF for moments can be readily seen in Fig. 6.8 in which the values of this DF are plotted against load level for the two loading sequences. It can be seen that the patterns of DF-load curves are quite similar for the two loading cases. In both cases, the values of DF first increase with load level up to load layer No. 3, below which level the girder strains are within elastic limits and the load-deflection behaviour linear. When the loading is increased beyond load layer No. 3, the values of the maximum DF start dropping until the loading is at the level of load layer No. 5, beyond which the values of DF, more or less, level off.

There can be different explanations for the increase in the maximum DF values with the increase of load while still being within the range of linear behaviour. The most plausible seems to be the one which relates to the stiffening of the most heavily loaded girder by the bearing restraint force. Since the bearing restraint force is likely to have the maximum value for the most heavily loaded girder, it is expected to stiffen this girder most which, in turn, attracts more load, and under a higher load, develops an even larger bearing restraint force, and so on.

If the peak values of maximum DF, i.e. those corresponding to load at the level of layer No. 3, are used as the elastic behaviour values, then the transverse redistribution of force effects can be shown to reduce these values by 16.4% and 19.3% for loadings in southern and northern segments, respectively. It is obvious that for the kind of bridge under consideration, the ultimate limit state affects large enough reductions in the maximum values of DF for moments, and hence in the maximum values of live load moments themselves, that they should not be ignored especially in the evaluation of existing bridges.

Neutral Axis Positions

Having calculated approximately the bearing restraint forces, the distances $\bar{y}$ of the neutral axis from the bottom flanges of girders were calculated by using Eg. (6.11) in which σ_B' and σ_T' are replaced by σ_b' and σ_t', respectively, and σ_{as} corresponded to individual girders. The various observations regarding the positions of the neutral axis calculated in this manner are given in the following.

It was found that the ignoring of the bearing restraint effect always led to lower positions of the neutral axis than those which are obtained by taking account of these effects. This observation is illustrated in Fig. 6.9 (b) which shows the positions of the neutral axis in all girders due to one particular load case, as obtained by these two procedures. It can be seen that the procedure which ignores the effects of bearing restraint leads to the position of the neutral axis for girder No. 6 well below the neutral axis of the steel girder alone. Such an outcome, which clearly cannot be real, is enough to invalidate this procedure.

The position of load was found to have an influence on the positions of the neutral axis but the influence was not a significant one, as can be seen in Fig. 6.9 (c). In this figure, the neutral axis positions are plotted for the various girders for the same level of loading in the two loading sequences. As expected, the neutral axis is slightly higher when a girder carries a directly applied load.

The effect of the level of load can be seen in Fig. 6.9 (d) for three particular load cases. A complete picture of this effect can be seen in Fig. 6.10 in which variations of the position of the neutral axis is plotted against load level for all cases. It can be seen in this figure that the neutral axis of the two outer girders, i.e. girder Nos. 1 and 6, are very close to the neutral axis of the naked steel girder. This obvious lack of composite action over these girders is clearly caused by the deterioration of concrete, which was observed over these girders, and a consequent loss of bond between the top flanges and concrete.

For the other girders which carried the applied loading directly, the position of the neutral axis generally moved towards the top flange with increase in the load during the initial stages of loading. However, as the load approached the failure load to the girder, the neutral axis moved towards that of the naked steel girder. The important conclusion drawn from this observation is that at the ultimate limit state, the bond between steel and concrete alone cannot be relied upon to provide any degree of composite action between the girder and deck slab.

7. Summary of Conclusions

Global and Local Failure

It was found that a girder continued to carry loads long after the formation of first yield; further, the overall bridge continued to carry loads long after the failure of the first girder.

The ratio of global and local failure loads, given in Table 5.3, were found to be substantially different for the two loading sequences, emphasizing the random nature in which the bridge behaved.

Cracking of the Deck Slab

The test has shown that at the failure of the bridge under a load which causes the girders to deflect unequally, the deck slab develops a crack pattern which is not usually accounted for in the design. It has been shown that the cracks in the deck slab, the patterns for which are shown in Figs. 5.4 and 5.5, are caused due to presence of composite action between the slab and girders, which eventually deteriorates as the load approaches the failure load.

Bearing Restraint Force

The bearing restraint force acting mainly at the interface of the bottom flanges of girders and the surface at which they rest, can be caused by either friction between the two surfaces or by restraint to the movement of bottom flanges provided by closely fitting ballast walls. When the cause is the former, as is usually the case, the reduction in applied moments decreases in magnitude with increase in the level of load.

In the Stoney Creek bridge, the applied moments were reduced by the bearing restraint forces by a minimum of about 11%.

The coefficient of friction between the somewhat rusted bottom flanges and the concrete abutment was found to be effectively equal to nearly 1.0 at the ultimate limit state.

The neglect of bearing restraint forces in the calculation of girder moments from observed strains necessarily leads to a significant under estimation of these responses.

Load Distribution at Service Loads

For loads within the linear range of bridge behaviour, the distribution characteristics of the bridge seemed to deteriorate slightly with the increase of load. As shown in Fig. 6.8, the distribution factor for mid-span moments in the most heavily load girder increased with load level during the initial stage of loading.

Load Distribution at the Ultimate Limit State

It was found that the transverse load distribution pattern at the ultimate limit state does not become so uniform as to distribute the loads evenly to the girders which are most remote from the load. However, the redistribution of moments within the immediately loaded girders is enough to reduce significantly the distribution factors for maximum girder moments. For the Stoney Creek Bridge, the distribution factor for maximum girder moment at the ultimate limit state was smaller than that under a very small load by about 12.5% in one loading sequence and by about 5.5% in the other. A more complete picture of the effect of load level on this distribution factor can be seen in Fig. 6.8.

It is noted that the six-bridge girder carried the uniformly distributed load directly over four consecutive girders including an outer one, as shown in Figs. 4.4 and 4.7. The outer girder remote from the applied loading hardly carried any load even at failure.

Composite Action

It has been shown conclusively that in the absence of mechanical shear connection between the deck slab and girders, any composite action between these two components which may exist under service loads, deteriorates rapidly as the load approaches the failure loads. Therefore, it can be concluded confidently that in slab-on-girder bridges without mechanical shear connection, any composite action should be ignored completely in strength calculations at the ultimate limit state.

9. References

[1] Bakht, B. (1988 a) "Testing of an Old Short Span Slab-on-Girder Bridge," SRR-88-01, MTO, Downsview, Ontario.

[2] Bakht, B. (1988 b) "Observed Behaviour of a New Medium Span Slab-on-Girder Bridge," SRR-88-02, MTO, Downsview, Ontario.

[3] Bakht, B. and Jaeger, L.G. (1988) "Support Restraint in Slab-on-Girder Bridges," ASCE Journal of Structural Engineering. To be published.

Table 5.1 Longitudinal strains in girders at mid-span due to loading in the southern segment of the bridge.

Girder No.	Gauge No.	Strain in mm x 10^6/mm at the End of Loading in Layer No.						
		1	2	3	4	5	6	7
1	61	-99	-215	-355	-562	-1193	-4056	-5707
	62	-18	-47	-76	-132	-343	-882	-1084
	63	125	249	375	534	800	1158	1336
2	64	4	10	24	-21	-423	-1649	-2598
	65	71	145	229	253	74	-271	-96
	66	181	372	571	724	917	1941	11433
3	67	-20	-38	-52	-66	-120	-594	-1082
	68	46	90	147	206	224	-50	-195
	69	147	298	457	633	811	1031	1132
4	70	-29	-63	-92	-121	-148	-234	-439
	71	16	28	44	78	130	145	39
	72	89	176	272	392	577	806	939
5	73	-45	-93	-132	-165	-216	-220	-204
	74	-1	-13	-15	-14	-20	-13	-36
	75	52	96	146	201	274	368	376
6	76	-26	-47	-60	-70	-69	1	51
	77	-15	-26	-29	-34	-26	29	59
	78	8	28	46	59	68	9	-46

Notes:

1) Each layer of load had 24 concrete blocks except layer No. 7 which had only 9 blocks.

2) Each concrete block weighed an average of about 9.26 kN.

3) For locations of gauges see Fig. 4.2, and for load positions Fig. 4.4.

4) Tensile strains are shown as the +ve.

Table 5.2 Longitudinal strains in girders at mid-span due to loading in the northern segment of the bridge.

Girder No.	Gauge No.	Strain in mm x 10^6/mm at the End of Loading in Layer No.						
		1	2	3	4	5	6	7
1	61	12	14	24	41	65	115	150
	62	-1	-5	-5	0	4	26	52
	63	-12	-24	-30	-42	-57	-84	-117
2	64	-2	-2	-10	-22	-38	-63	-76
	65	7	25	40	47	66	73	77
	66	40	57	97	127	189	269	380
3	67	-21	-37	-49	-58	-74	-92	-54
	68	18	42	69	111	154	221	414
	69	91	180	277	395	553	787	791
4	70	-53	-93	-139	-270	-398	-433	-562
	71	29	60	84	77	52	59	-36
	72	154	281	406	558	679	723	734
5	73	-129	-186	-231	-229	-279	-645	-789
	74	20	77	152	345	620	570	242
	75	229	457	708	2228	10476	12235	12370
6	76	-144	-289	-435	-600	-812	-1249	-1307
	77	-31	-56	79	69	-3	89	108
	78	175	353	513	555	527	512	564

Notes:

1) Each layer of load had 24 concrete blocks except layer No. 7 which had 11 blocks.

2) Each concrete block weighed an average of about 9.26 kN.

3) For location of gauges see Fig. 4.2, and for load positions Fig. 4.7.

4) Tensile strains are shown as +ve.

Table 5.3 Relationships between local and overall failure loads.

Loading In...	Southern Segment	Northern Segment
$\frac{\text{Failure load for the bridge}}{\text{Load causing first yield in a girder}}$	1.40	2.10
$\frac{\text{Failure load for the bridge}}{\text{Load causing failure in the first girder}}$	1.15	1.60
$\frac{\text{Failure load of an external girder}}{\text{Load causing yield in an external girder}}$	1.20	*
$\frac{\text{Failure load of an internal girder}}{\text{Load causing yield in an internal girder}}$	1.45	1.30

*Girder No. 6 did not fail for loading in the northern segment.

Table 5.4 Mid-span deflections of girders.

Loading In...	Gauge No. (Girder No.)	Deflections in mm at Mid-span at the End of Loading in Layer No.						
		1	2	3	4	5	6	7
Southern Segment	87 (1)	7.06	14.66	22.80	34.35	55.67	101.20	101.24
	86 (6)	1.37	2.72	3.83	4.57	4.57	0.46	-3.75
Northern Segment	87 (1)	-0.40	-0.71	-1.35	-2.23	-3.69	-6.44	-7.81
	86 (2)	9.85	20.36	31.31	46.05	68.29	107.66	107.84

Notes:

1) Each layer of load had 24 concrete blocks except layer No. 7 which had 9 blocks for loading in the southern segment and 11 for loading in the northern segment.

2) Downward deflections are shown as +ve.

Table 5.5 Values of interface slip between the deck slab and top flanges of girders, near the eastern abutment.

Loading In...	Gauge No.	Interface Slip in mm Near East Support at the End of Loading in Layer No.						
		1	2	3	4	5	6	7
Southern Segment	80	0.40	0.82	1.35	2.09	3.80	9.09	14.36
	81	-0.07	0.00	0.24	0.49	1.05	3.09	4.00
	82	-0.07	-0.09	-0.09	-0.04	0.70	3.30	7.08
	83	0.11	0.19	0.32	0.55	1.03	2.71	4.40
	84	0.02	0.15	0.21	0.17	0.30	0.32	0.43
	85	0.03	0.03	0.05	-0.21	-0.61	-2.34	-4.76
Northern Segment	80	0.04	0.32	0.51	0.55	0.63	1.16	1.94
	81	-0.10	0.00	0.02	-0.05	0.02	0.00	-0.12
	82	-0.02	0.07	0.25	0.27	0.63	1.24	1.83
	83	0.13	0.51	0.88	1.30	2.65	5.21	8.69
	84	0.62	1.34	1.84	2.54	3.67	6.34	11.47
	85	0.82	1.28	1.28	1.27	0.39	-1.34	-4.24

Notes:

1) Interface slip is shown as +ve when the deck slab moves towards the abutment with respect to the top flange of the girder.

2) For gauge locations see Fig. 4.3.

Table 6.1 Total net moments in girders at mid-span.

Loading In...	Load Layer No.	Beam mt., M, kN m	$F\bar{y}$, kN m	M+$F\bar{y}$, kN m	Σ Computed girder mts. $\bar{M}$, kN m	$\frac{M+F\bar{y}}{M}$	$\frac{F\bar{y} \times 100}{M}$, %
Southern Segment	1	623	-99	524	525	1.00	-15.9
	2	1266	-194	1052	1052	1.00	-15.6
	3	1869	-289	1580	1603	0.99	-15.4
	4	2492	-368	2124	2151	0.99	-14.8
	5	3115	-402	2713	2713	1.00	-12.9
	6	3738	-409	3329	3329	1.00	-10.9
Northern Segment	1	623	-78	545	544	1.00	-12.5
	2	1246	-169	1077	1089	0.99	-13.6
	3	1869	-245	1624	1638	0.99	-13.1
	4	2492	-418	2074	2102	0.99	-16.8
	5	3115	-5513	2562	2412	1.06	-17.8
	6	3738	-557	3181	3170	1.00	-14.9

Table 6.2 Distribution factors for girder moments at mid-span.

Loading In...	Load Layer No.	Distribution Factors For Mid-span Moment In Girder No.					
		1	2	3	4	5	6
Southern Segment	1	1.22	2.32	1.80	1.03	0.48	0.13
	2	1.19	2.40	1.84	0.98	0.41	0.16
	3	1.14	2.43	1.86	1.03	0.39	0.15
	4	1.15	2.23	1.91	1.11	0.47	0.12
	5	1.03	2.03	1.94	1.34	0.54	0.12
	6	0.86	2.03	2.03	1.46	0.60	0.01
Northern Segment	1	-0.07	0.40	0.88	1.44	1.98	1.37
	2	-0.08	0.32	0.85	1.35	2.13	1.42
	3	-0.07	0.33	0.91	1.27	2.23	1.33
	4	-0.07	0.34	1.07	1.36	2.21	1.09
	5	-0.07	0.44	1.07	1.60	1.87	1.09
	6	-0.07	0.46	1.08	1.79	1.87	0.95

(a) A view showing the wood plank sidewalk

(b) A view from the underside of the bridge

Figure 2.1/ Views of the Stoney Creek Bridge a few months before the test

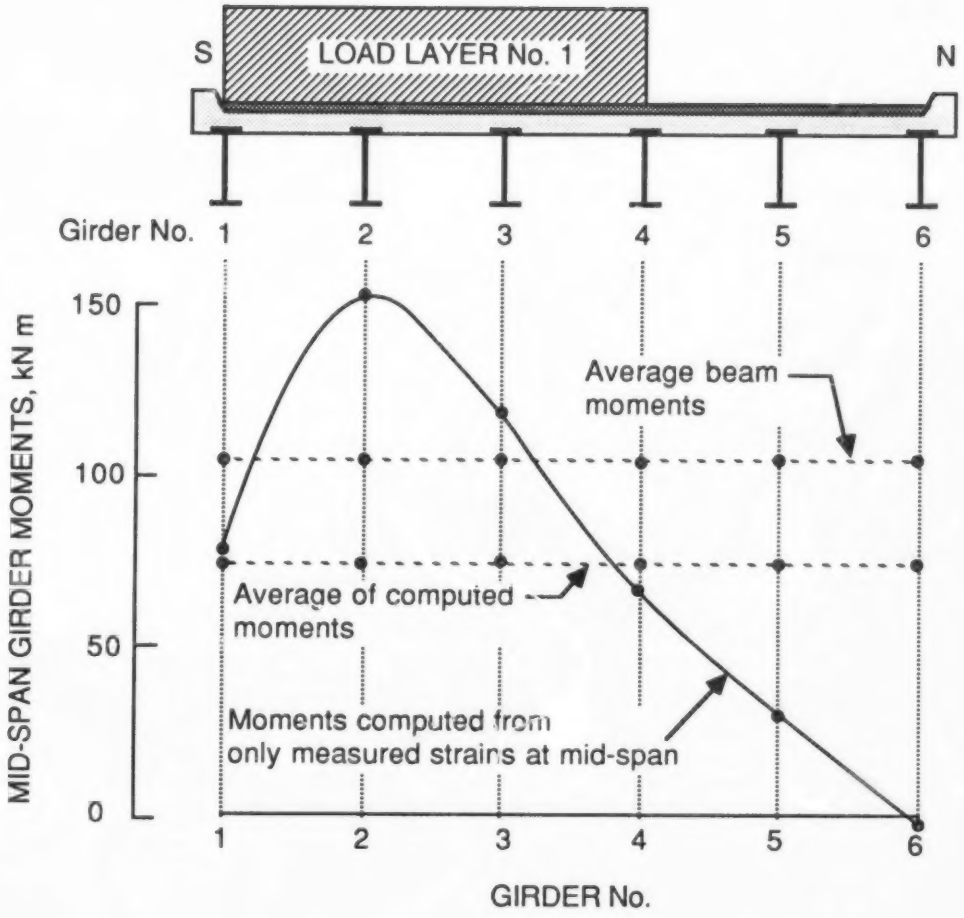

Figure 2.2/ Moments at mid-span due to one particular load case

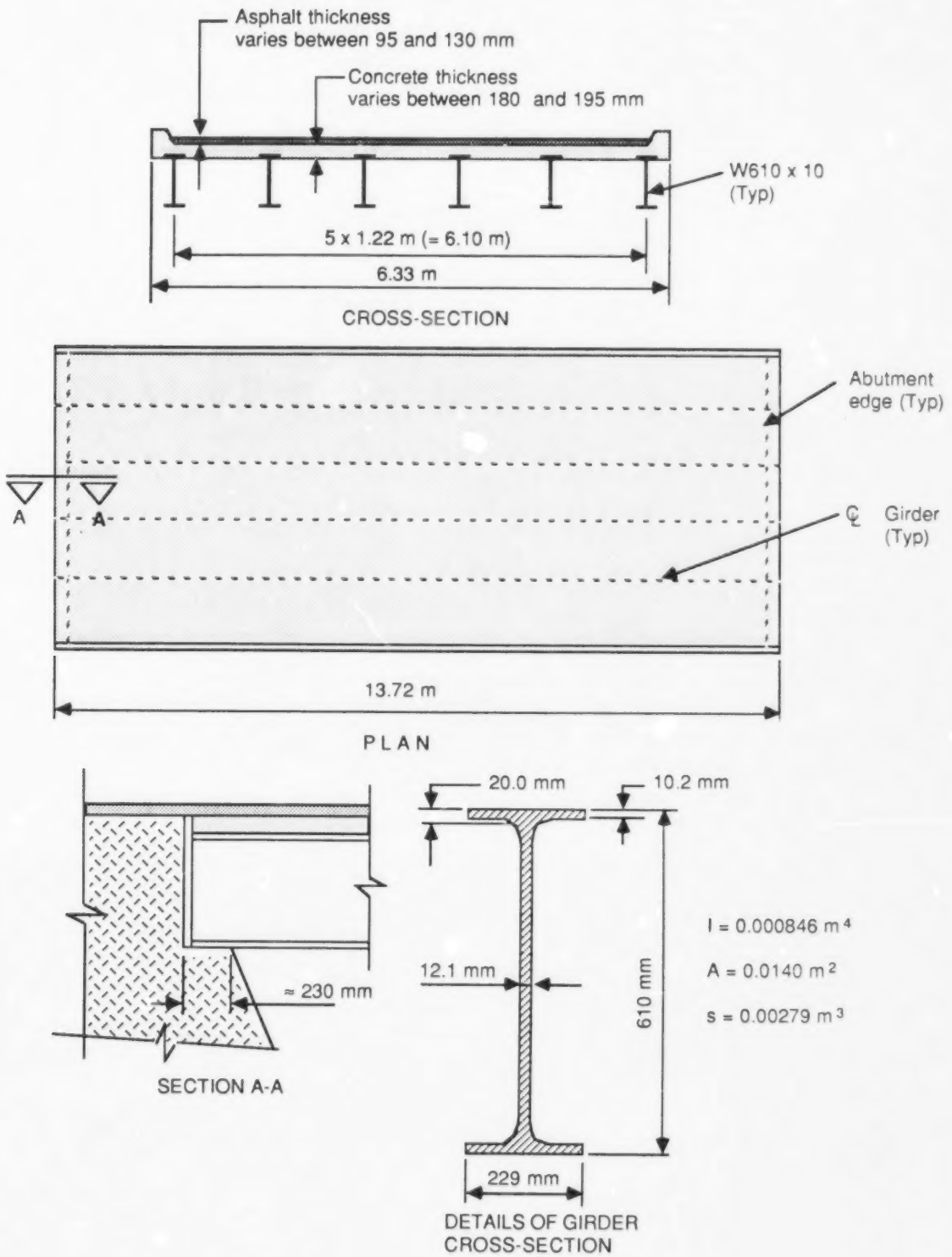

Figure 3.1/ Bridge details

Figure 4.1/ A view of the bridge showing a part of the temporary wood structure erected under the bridge

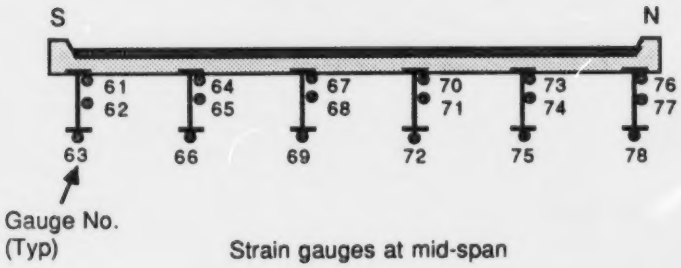

Strain gauges at mid-span

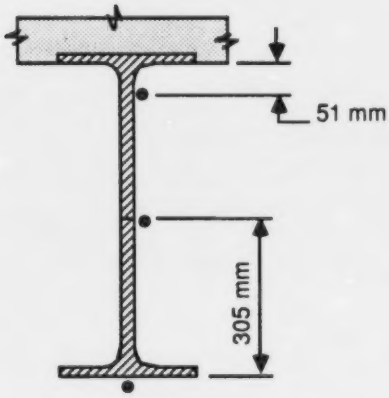

Typical gauge locations
on girders, at mid-span

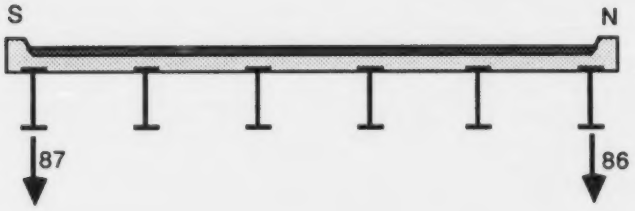

Deflection transducers near the mid-span

Figure 4.2/ Gauges at or near mid-span and their identifying numbers

Numbering sequence of slip transducers

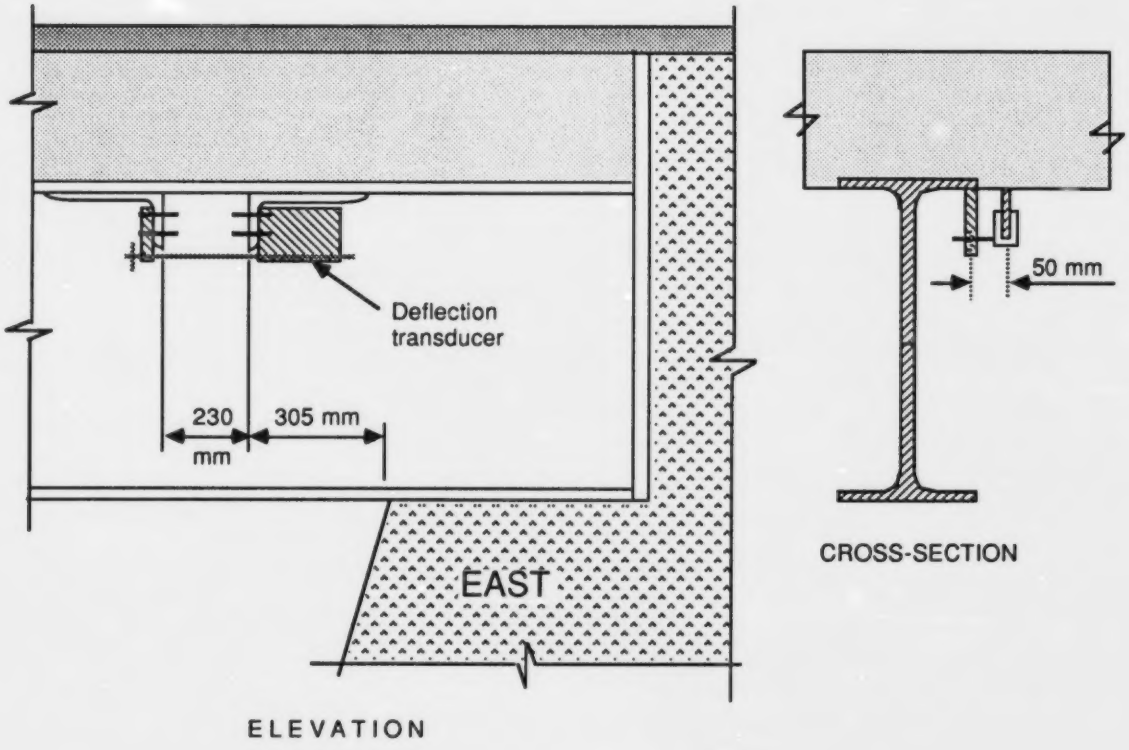

Details of a typical slip transducer

Figure 4.3/ Instruments for measuring interface slip

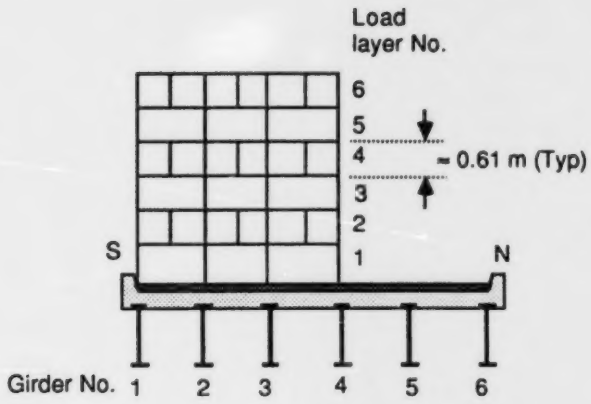

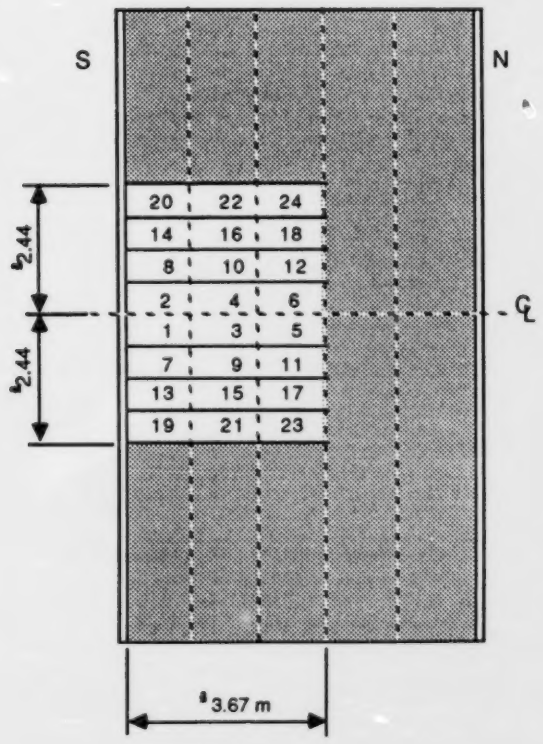

Loading sequence of concrete blocks on plan of odd-numbered load layers

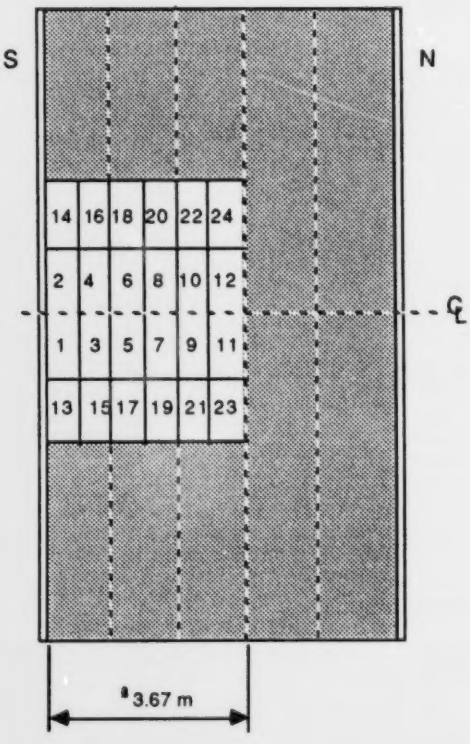

Loading sequence of concrete blocks on plan of even-numbered load layers

Figure 4.4/ Placing sequence of loading in the southern segment of the bridge

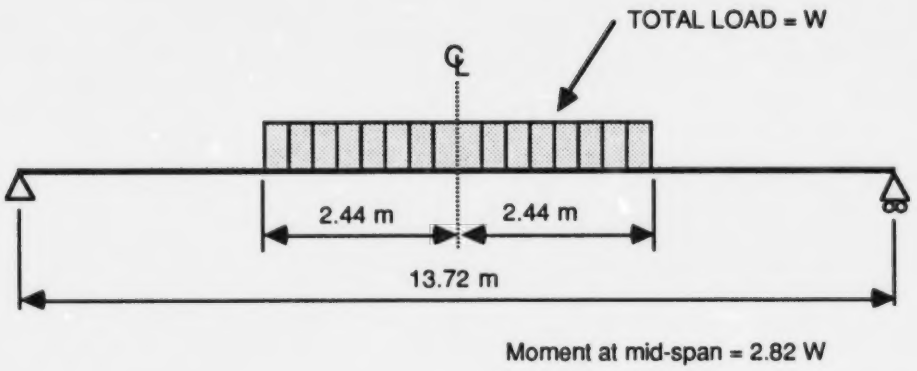

(a) Uniformly distributed loading

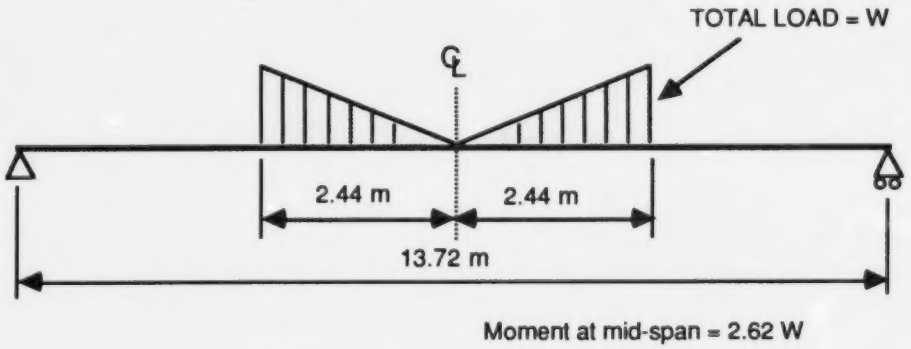

(b) Loading distributed in a double triangular form

Figure 4.5/ Beam moments at mid-span

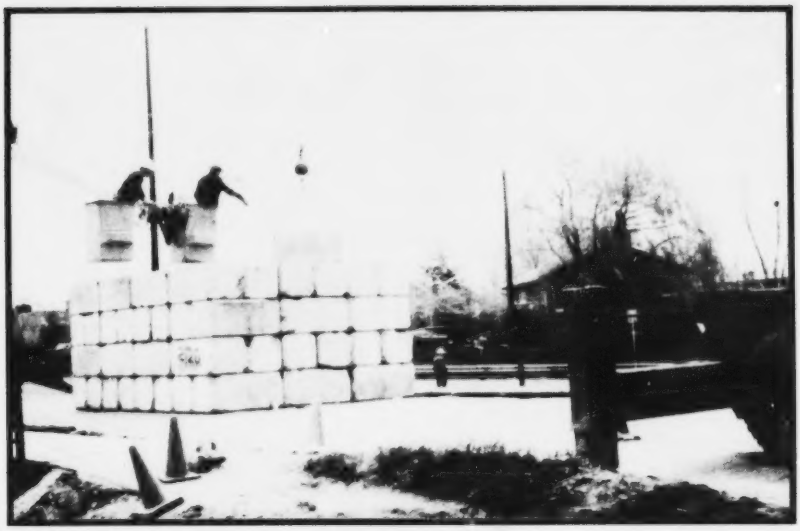

Figure 4.6/ Loading of the bridge with concrete blocks

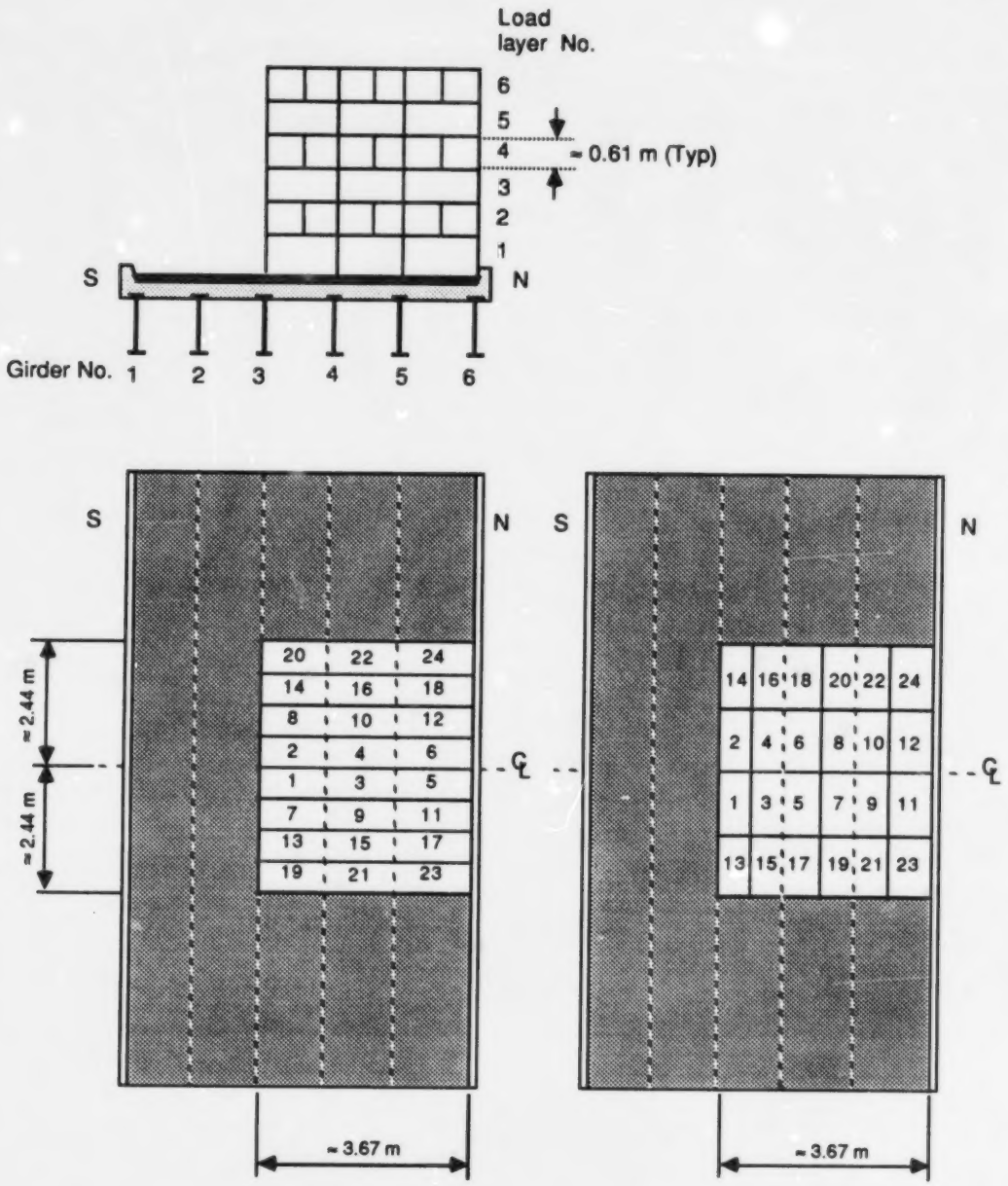

Loading sequence of concrete blocks on plan of odd-numbered load layers

Loading sequence of concrete blocks on plan of even-numbered load layers

Figure 4.7/ Placing sequence of loading in the northern segment of the bridge

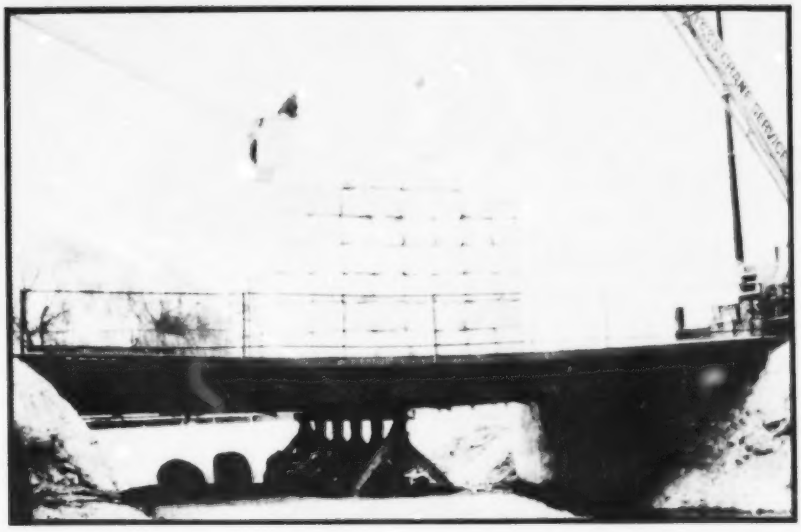

Figure 4.8/ Placing of concrete blocks in the 7th layer for loading in the southern segment

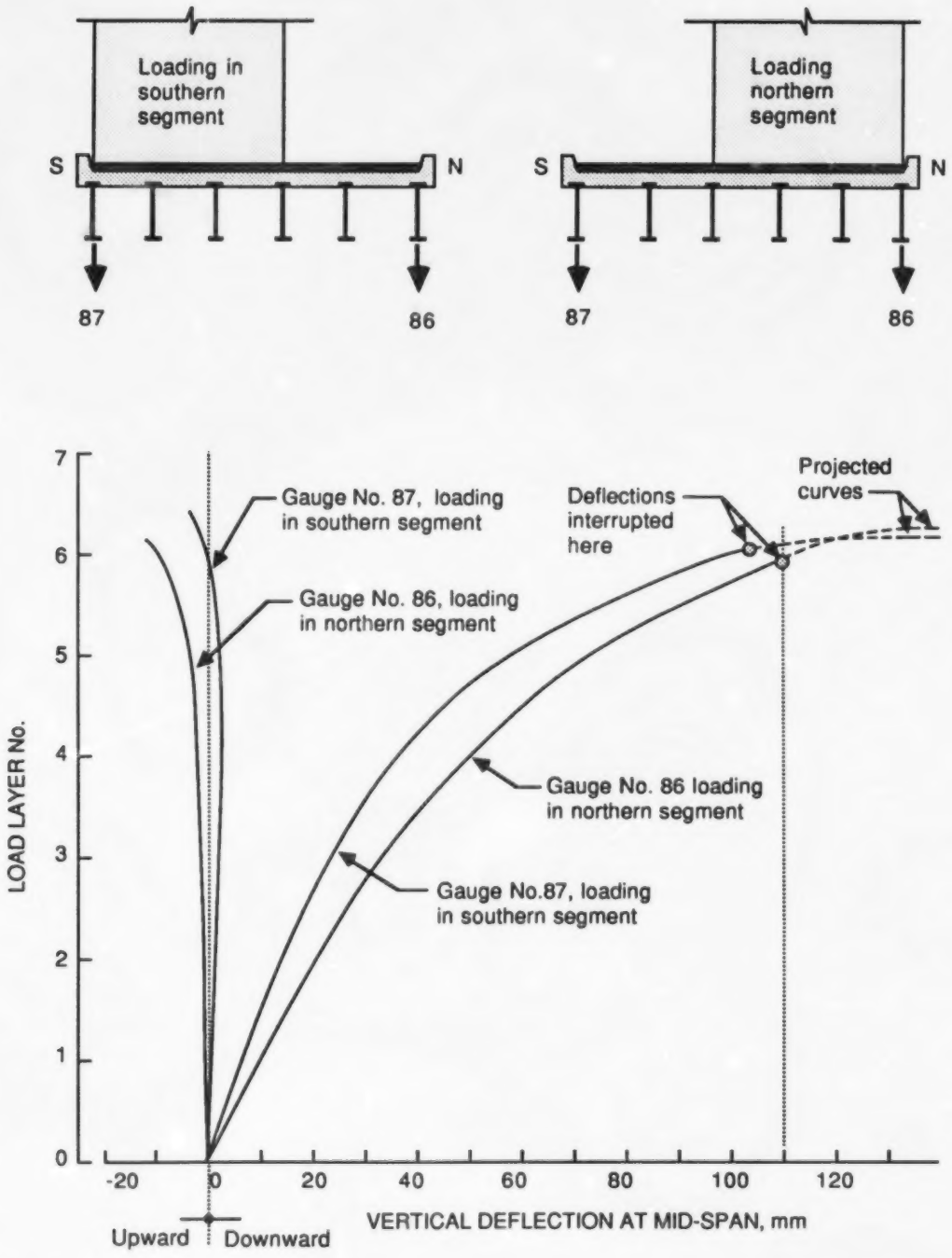

Figure 4.9/ Girder deflections at mid-span

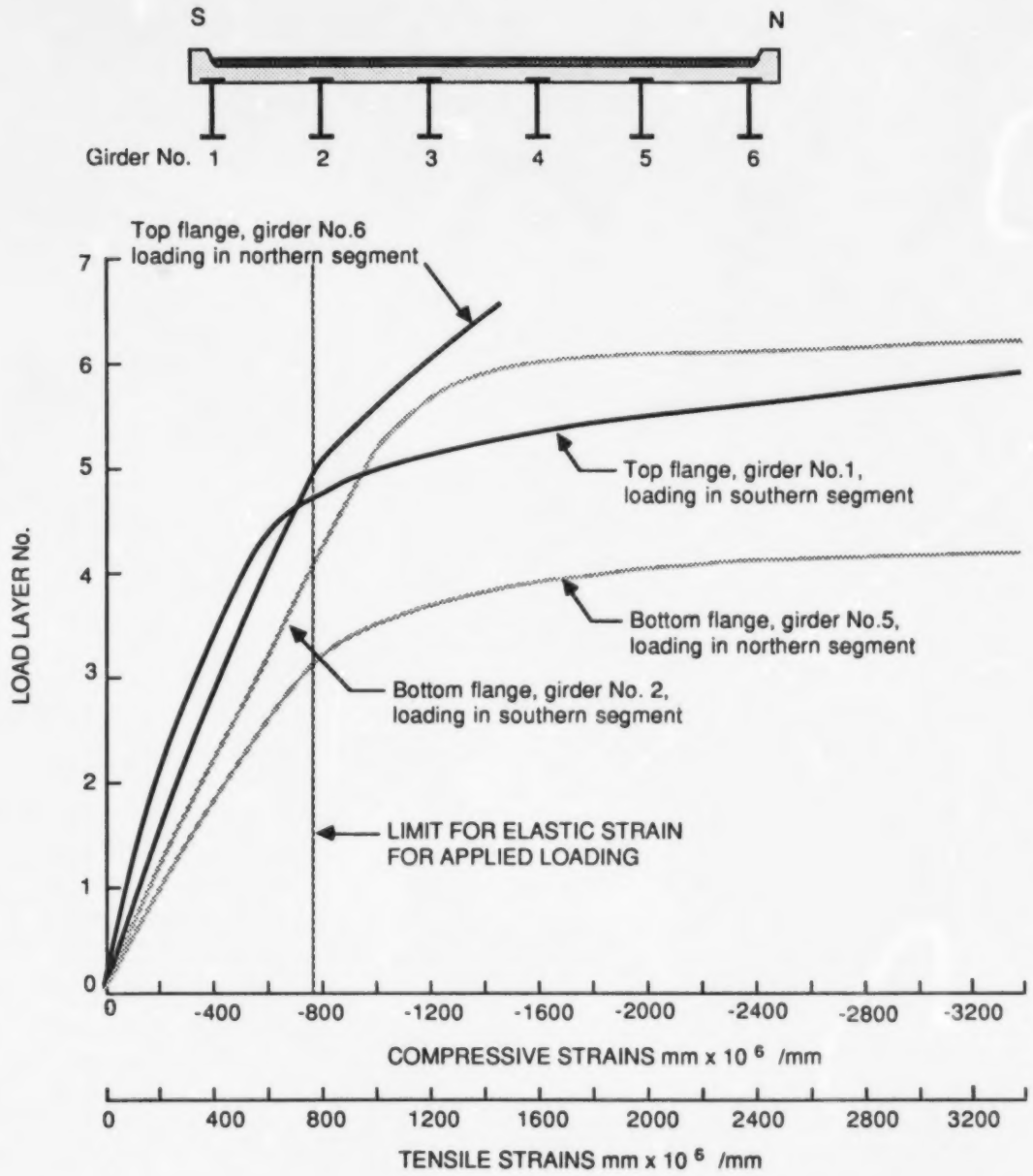

Figure 5.1/ Some girder strains plotted against load

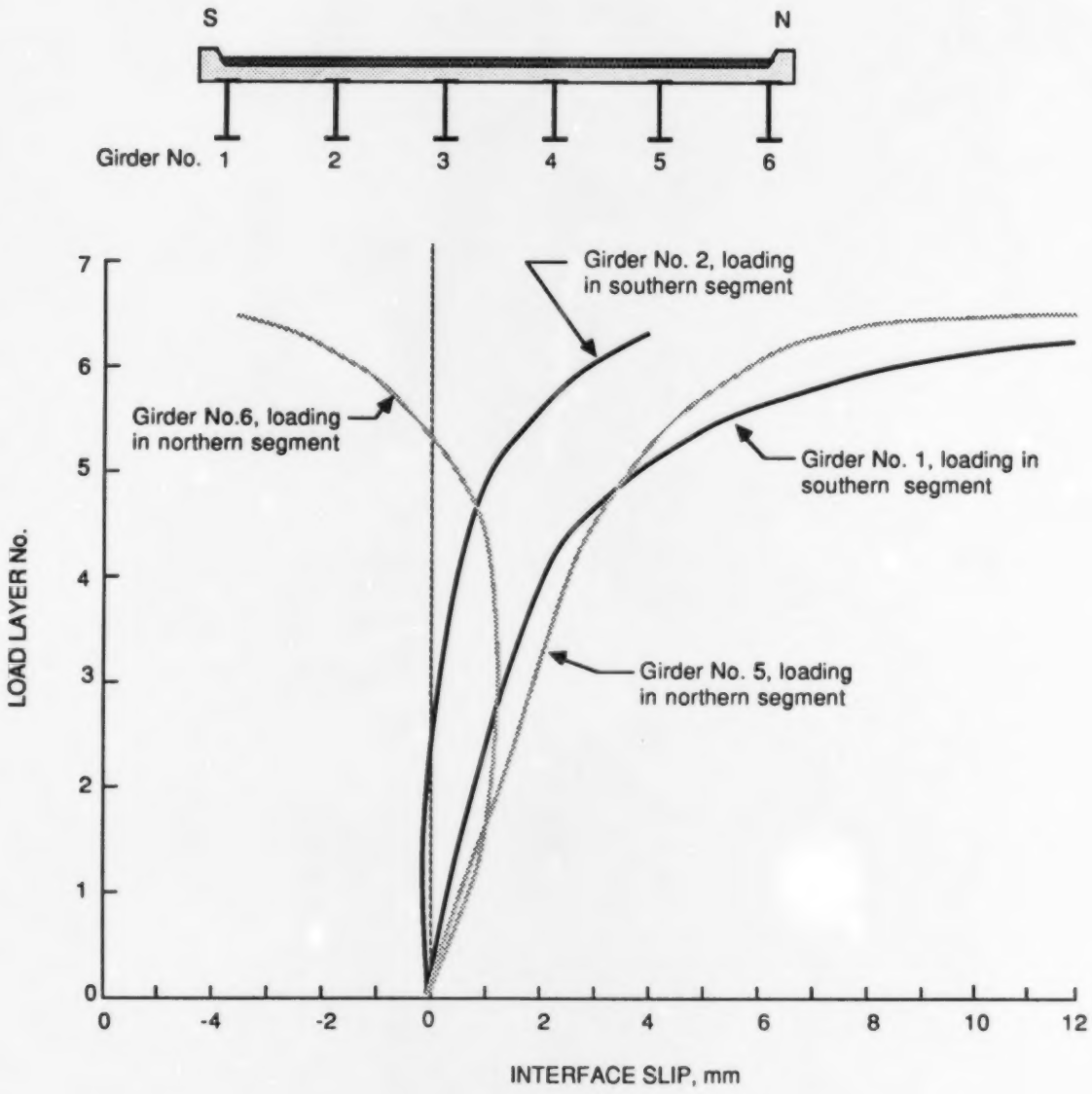

Notes: 1. The interface slip is shown as +ve when the deck slab moves towards the abutment with respect to the girder top flanges.

2. For gauge locations, see Fig. 4.3.

Figure 5.2/ Interface slip of deck slab with respect to the top flange of girders

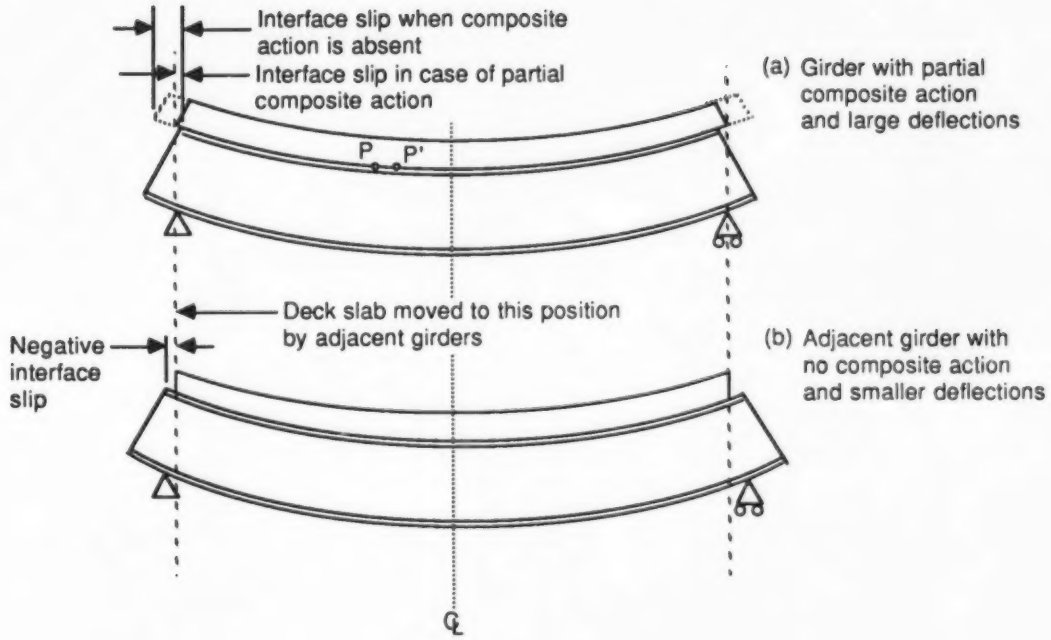
Interface slip when composite action is absent
Interface slip in case of partial composite action
(a) Girder with partial composite action and large deflections
P
P'
Deck slab moved to this position by adjacent girders
Negative interface slip
(b) Adjacent girder with no composite action and smaller deflections
℄

Figure 5.3/ Exaggerated representation of interface slip

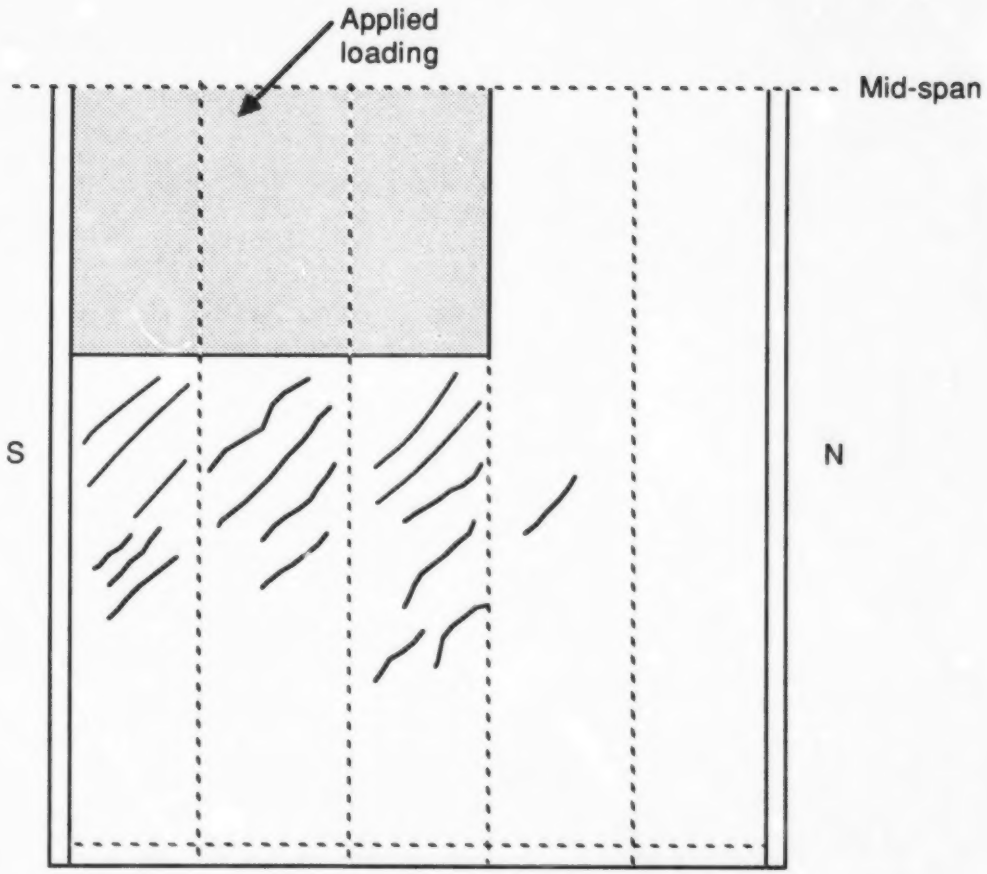

Notes: 1. Crack pattern was symmetrical about the mid-span line

2. Cracks on the underside of the slab, shown as viewed from the top

Figure 5.4/ Crack pattern due to ultimate load on the southern segment of the bridge

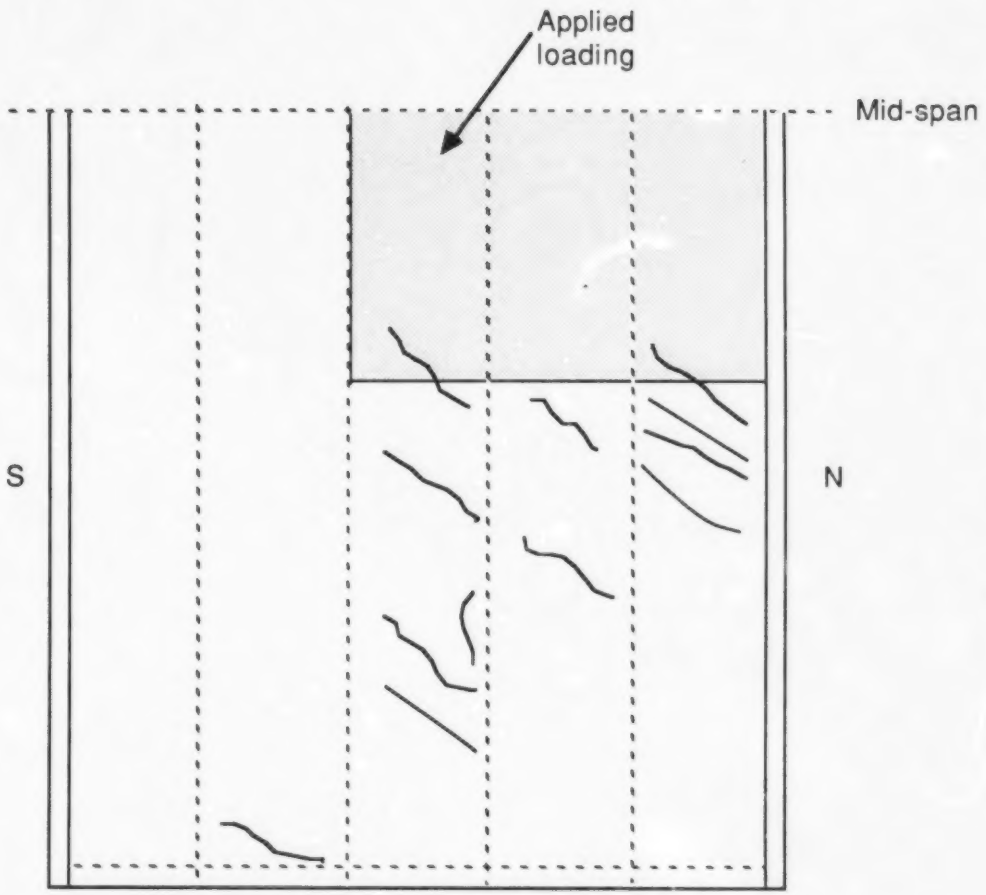

Notes: 1. Crack pattern was symmetrical about the mid-span line

2. Cracks on the underside of the slab, shown as viewed from the top

Figure 5.5/ Crack pattern due to ultimate load on the northern segment of the bridge

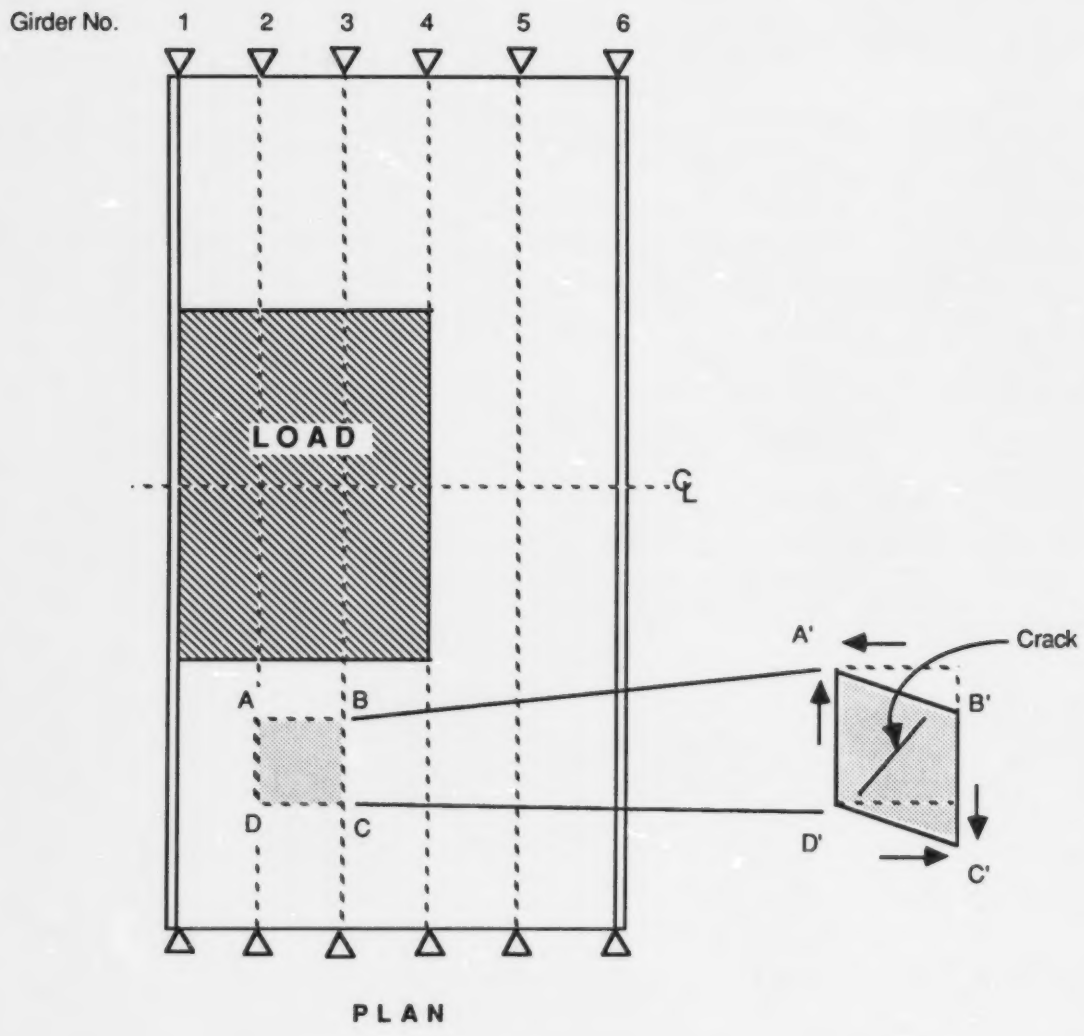

Figure 5.6/ An element of deck slab

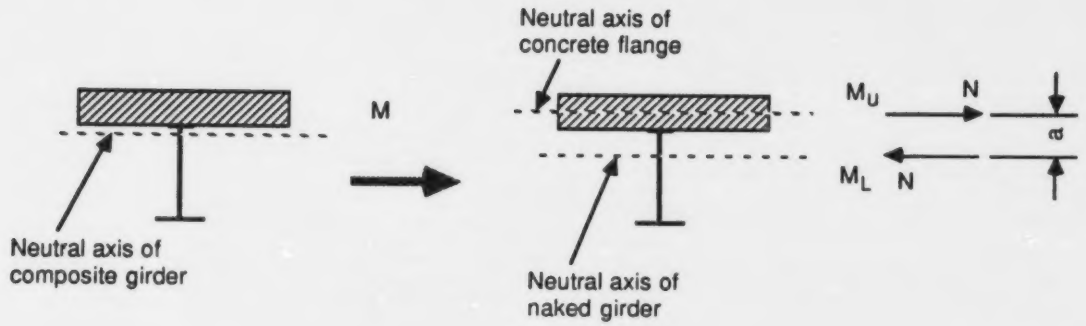

(a) Moments in a Composite Girder

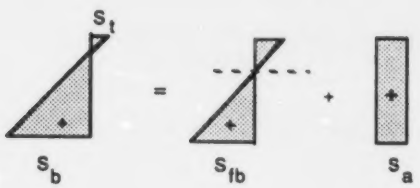

(b) Stresses in the Steel Girder without Axial Force Due to Bearing Restraint

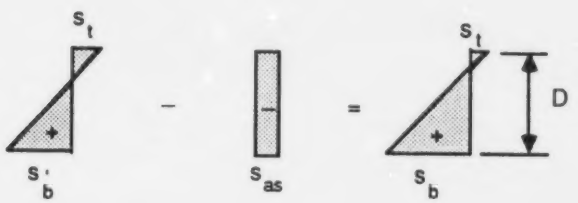

Stresses computed from observed strains

Average stress due to bearing restraint force

Net stresses due to flexure

(c) Obtaining Stresses due to Flexure when Axial Force due to Bearing Restraint is Present

Figure 6.1/ Calculation of girder moments from measured strains

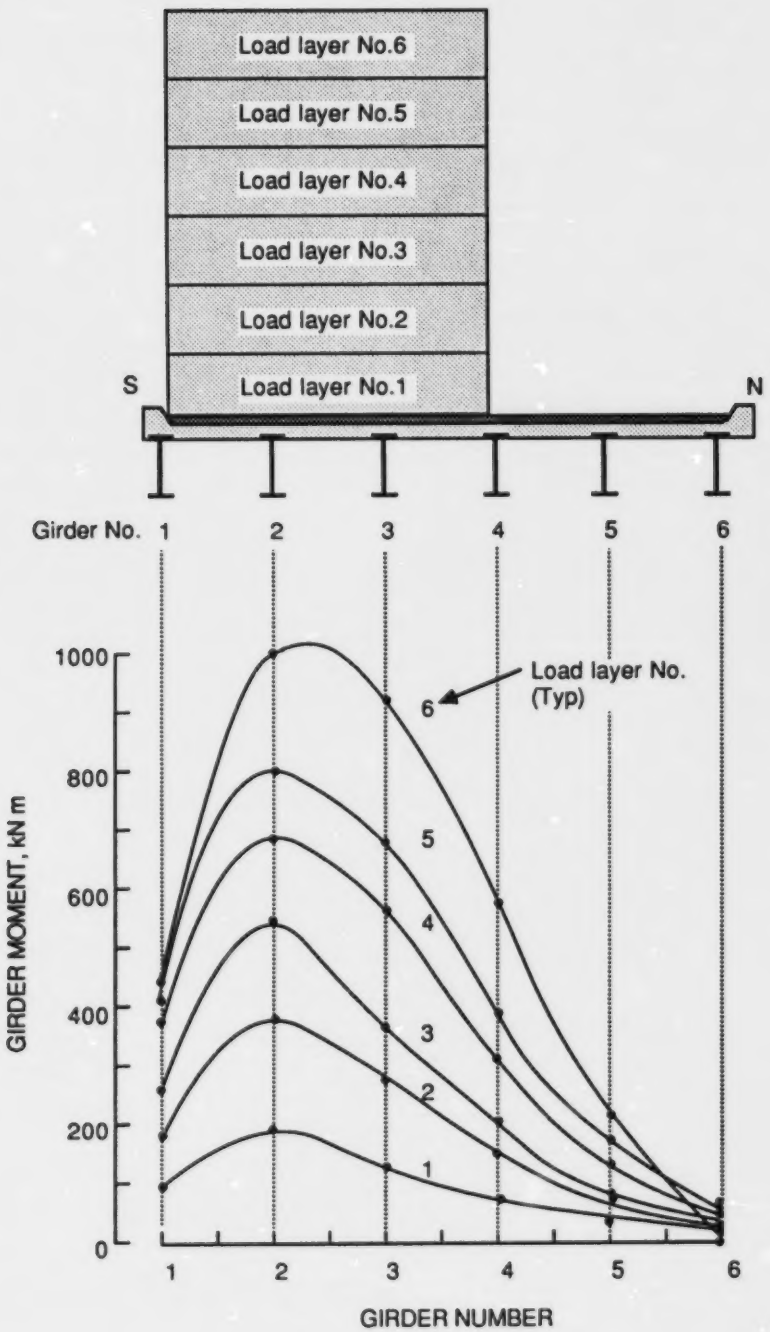

Figure 6.2/ Girder moments at mid-span due to loading in southern segment

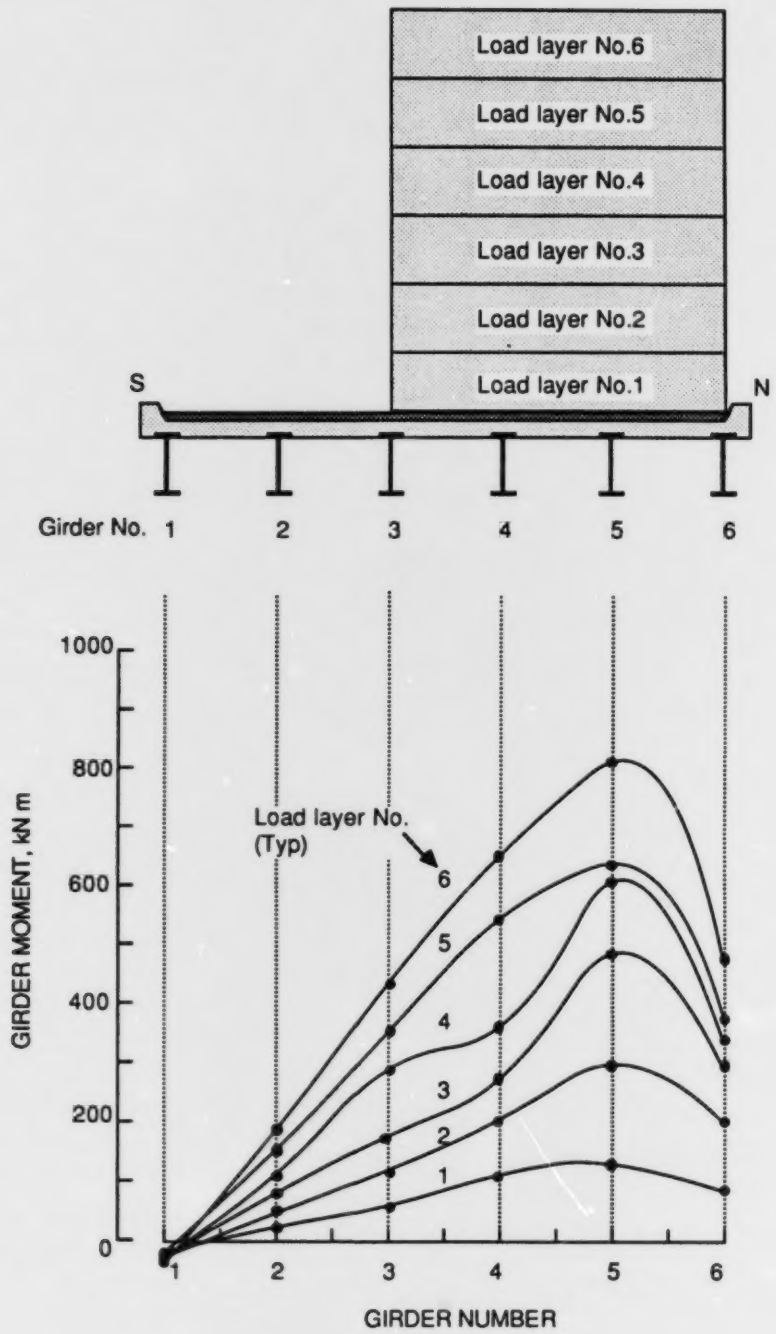

Figure 6.3/ Girder moments at mid-span due to loading in northern segment

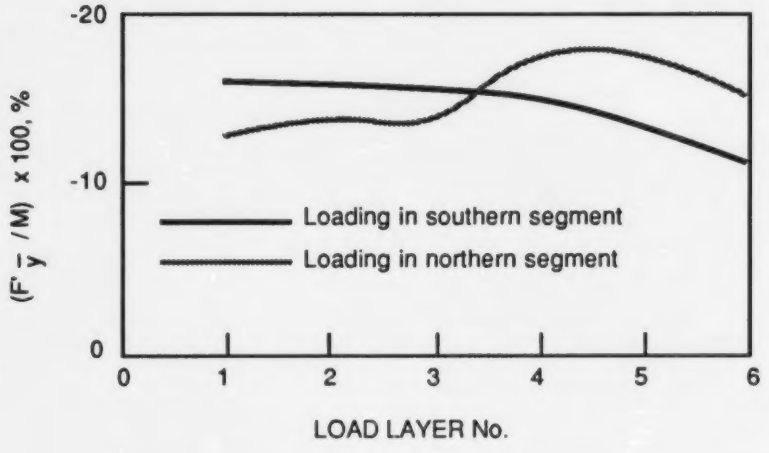

Figure 6.4/ Reduction of applied moments due to bearing restraint

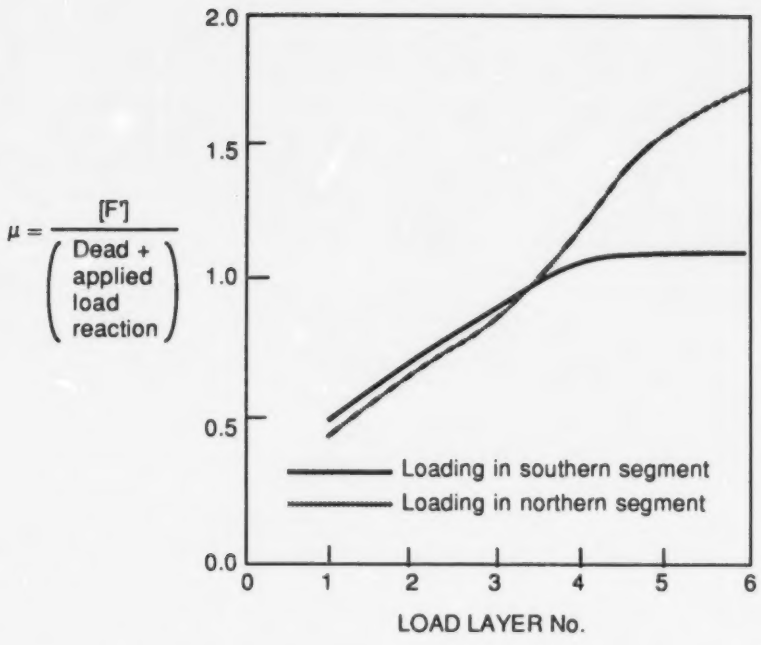

Figure 6.5/ Ratios of restraint force to total reaction

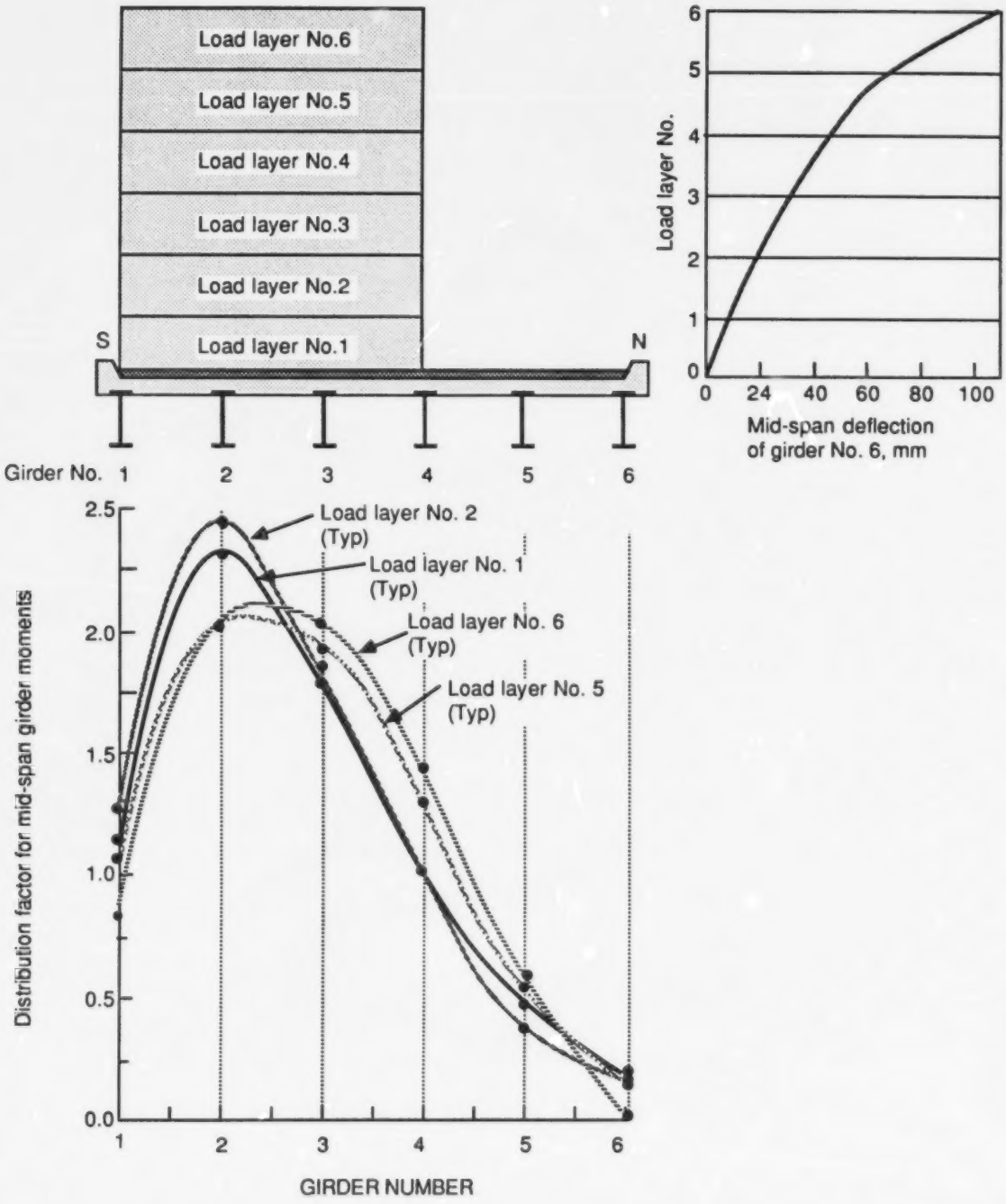

Figure 6.6/ Transverse distribution of girder moments due to loading in southern segment

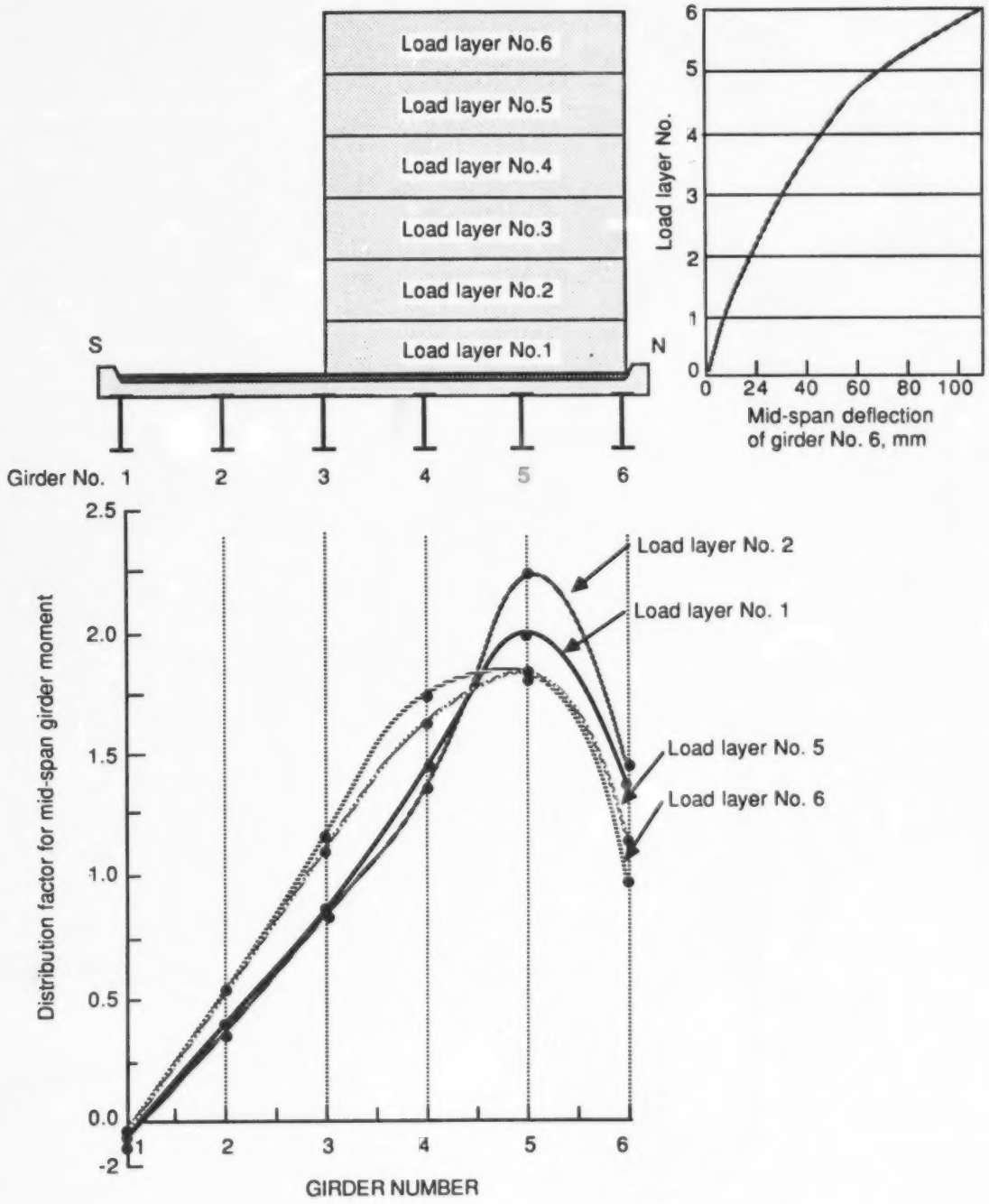
Load layer No.6
Load layer No.5
Load layer No.4
Load layer No.3
Load layer No.2
Load layer No.1
S
N
Girder No. 1 2 3 4 5 6
Load layer No.
0 1 2 3 4 5 6
0 24 40 60 80 100
Mid-span deflection of girder No. 6, mm
Distribution factor for mid-span girder moment
2.5 2.0 1.5 1.0 0.5 0.0 -2
Load layer No. 2
Load layer No. 1
Load layer No. 5
Load layer No. 6
1 2 3 4 5 6
GIRDER NUMBER

Figure 6.7/ Transverse distribution of girder moments due to loading in northern segment

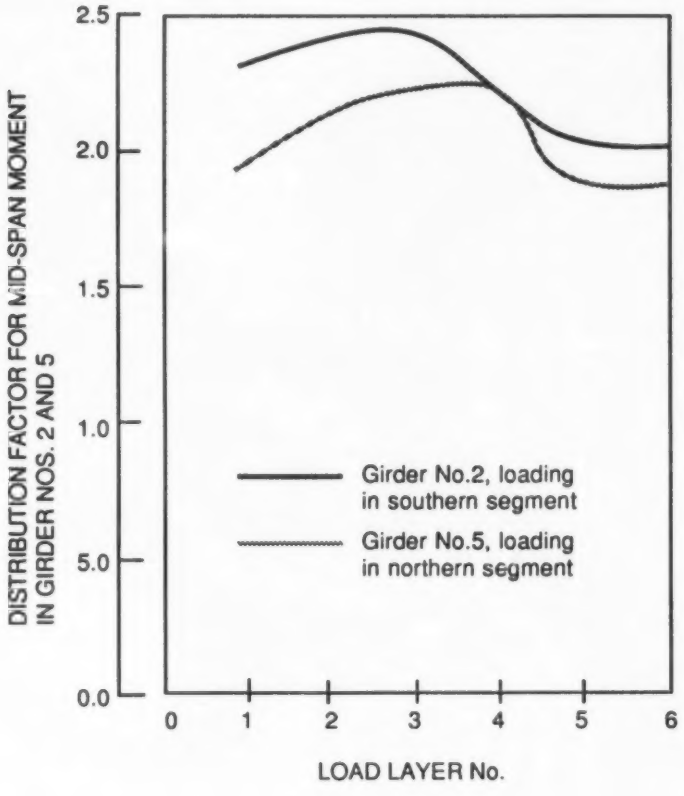

Figure 6.8/ Variation in values of maximum distribution factors for moments with respect to load level

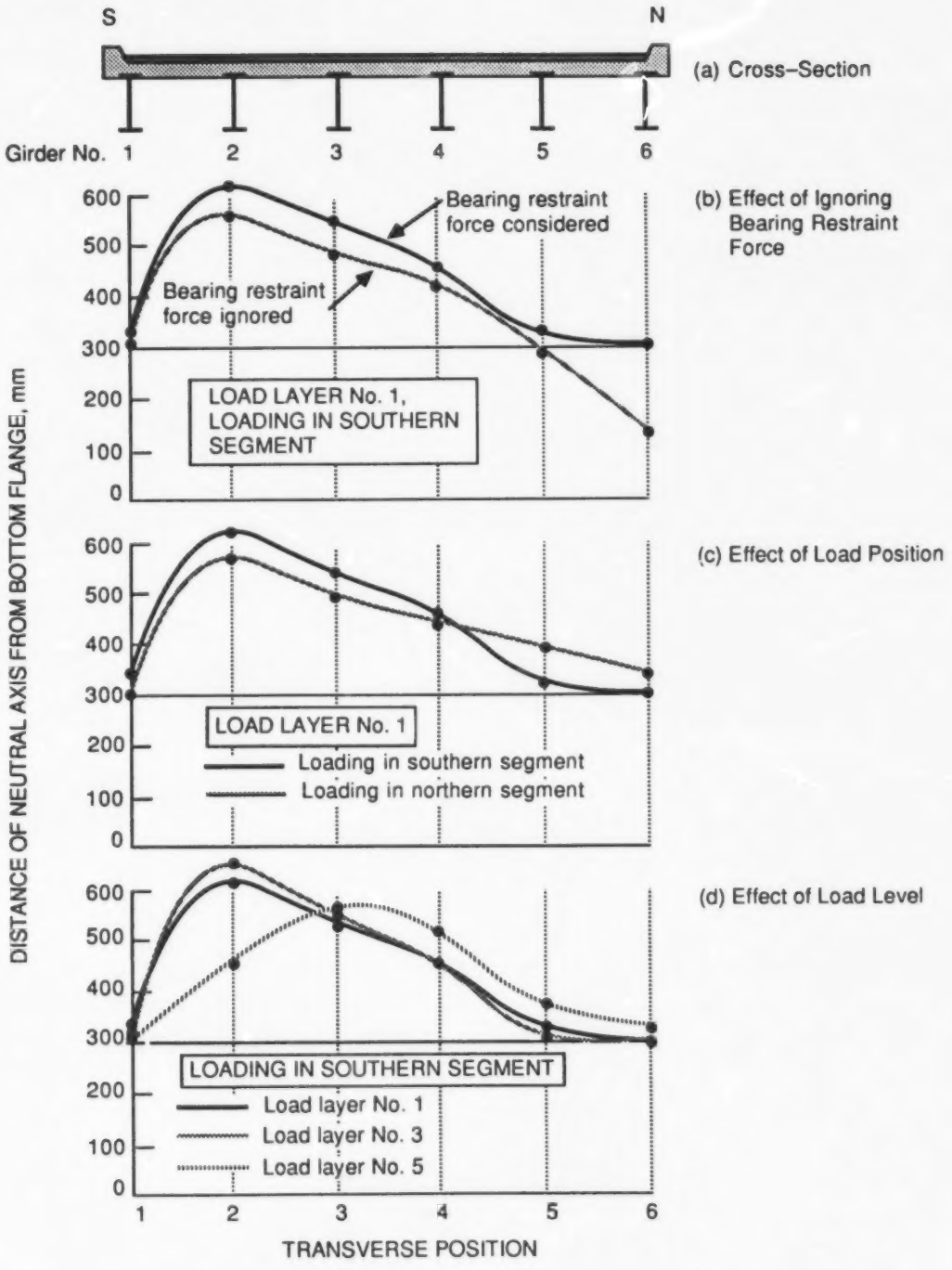

Figure 6.9/ Positions of neutral axes

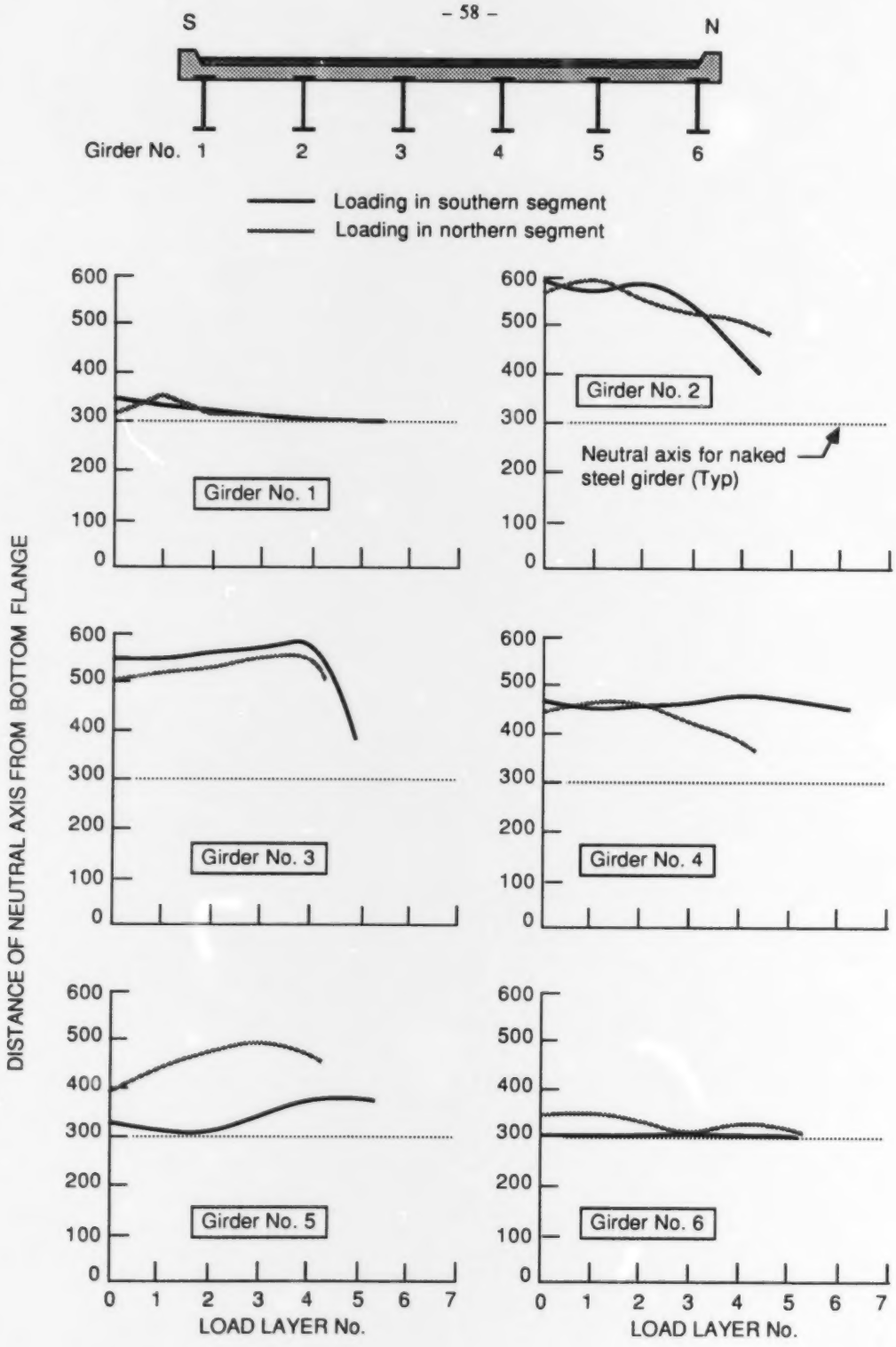

Figure 6.10/ Positions of neutral axes